Featured in Physics

Joint analysis of Dark Energy Survey Year 3 data and CMB lensing from SPT and Planck. III. Combined cosmological constraints

T. M. C.Abbott, ¹ M. Aguena² A. Alarcon, ³ O. Alves, ⁴ A. Amon, ^{5,6} F. Andrade-Oliveira, J. Annis, ⁷ B. Ansarinejad, ⁸ S. Avila, ⁹ D. Bacon, ¹⁰ E. J. Baxter, ¹¹ K. Bechtol, ¹² M. R. Becker, ⁸ B. A. Benson, ^{13,14} G. M. Bernstein, ¹⁵ E. Bertin, ^{16,17} J. Blazek, ¹⁸ L. E. Bleem, ^{19,14} S. Bocquet, ²⁰ D. Brooks, ²¹ E. Buckley-Geef, ^{3,7} D. L. Burke, ^{22,23} H. Camacho, ^{4,2} A. Campos, ⁵ J. E. Carlstrom, ^{14,26,27,19,13} A. Carnero Roseff, ^{8,29} M. Carrasco Kind, ^{9,31} J. Carretero, ² R. Cawthon, ³ C. Chang, ^{13,14} C. L. Chang, ^{13,14} C. L. Chang, ^{14,14,28} A. Choi, ³⁵ R. Chown, ^{36,37} C. Conselica, ^{33,39} J. Cordero, ⁸ M. Costanz, ^{40,41,42} T. Crawford, ⁴ A. T. Crites, ^{4,13,43} M. Crocce, ^{4,45} L. N. da Costa, ² C. Davis, ² T. M. Davis, ⁶ T. de Haaff, ^{7,48} J. De Vicente, ⁸ J. DeRose, ⁸ S. Desaf, ¹ H. T. Diehl, ⁷ M. A. Dobbs, ^{52,53} S. Dodelson, ^{25,54} P. Doel, ¹ C. Doux, ^{15,55} A. Drlica-Wagner, ^{37,7,14} K. Eckert, ¹⁵ T. F. Eifler, ^{65,57} F. Elsner, ¹ J. Elvin-Poole, ^{85,9} S. Everett, ⁷ W. Everett, ⁹ X. Fang, ^{61,56} I. Ferrero, ⁶² A. Fert, ⁵⁷ B. Flaugher, P. Fosalbå, ⁴⁵ O. Friedrich, J. Friemari, ¹⁴ J. Garcia-Bellido, M. Gatti, ¹⁵ E. M. George, ³ T. Giannantonio, ⁶ G. Giannini, ³² D. Gruend, ^{30,31} J. Gschwend, ⁶⁴ G. Gutierrez, N. W. Halverson, ^{85,56} J. D. Hrubes, ^{87,70} H. Huang, ^{56,73} E. M. Huff, ⁵⁷ D. Huterer, B. Jain, ¹⁵ D. J. James, ⁴ M. Jarvis, ⁵ T. Jeltema, ⁴ S. Kent, ^{7,14} L. Knox, ⁷⁵ A. Kovacs, ^{38,29} E. Krause, ⁶ K. Kuehn, ^{76,77} N. Kuropatkin, ⁷ O. Lahav, ² A. T. Lee, ^{48,78} P.-F. Leget, ²² P. Lemos, ^{21,79} A. R. Liddle, ⁸⁰ C. Lidman, ^{81,82} D. Luong-Var, ² J. J. McMahon, ^{14,13,26,27} N. MacCrant, ³ M. March, ¹⁵ J. L. Marshall, ⁸⁴ P. Martini, ^{38,85,86} J. McCullough, ²² P. Melchior, ⁸⁷ F. Menanteau, ³¹ S. S. Meyer, ^{41,13,26,27} R. Miquel, ^{88,29} L. Prati, ^{31,4} S. Pande, ⁵⁷ Y. Park, ⁶⁸ F. Paz-Chinchon, ⁵⁰ M. E. S. Pereir, ⁵⁸ A. R. Pier

(DES and SPT Collaborations)

¹Cerro Tololo Inter-American Observatory. NSF's NationalOptical-Infrared Astronomy Research Laborato@asilla 603, La Serena, Chile ²Laboratório Interinstitucional de e-Astronomia-LlneA, Rua Gal. José Cristino 77, Rio de Janeiro, RJ-20921-400 Brazil ³Argonne NationalLaboratory, 9700 South Cass Avenubemont, Illinois 60439, USA ⁴Departmentof Physics,University of Michigan, Ann Arbor, Michigan 48109,USA ⁵Institute of Astronomy University of Cambridge, Madingley Road Cambridge CB3 0HA United Kingdom ⁶Kavli Institute for CosmologyUniversity ofCambridge, Madingley Road Cambridge CB3 0HAUnited Kingdom ⁷Fermi National Accelerator Laboratory P. O. Box 500, Batavia, Illinois 60510, USA Schoolof Physics, University of Melbourne, Parkville VIC 3010, Australia ⁹Instituto de Fisica Teorica UAM/CSIQJniversidad Autonoma de Madrid∕8049 Madrid,Spain ¹⁰Institute of Cosmology and Gravitation University of Portsmouth, Portsmouth PO1 3FXUnited Kingdom ¹¹Institute for Astronomy, University of Hawai'i, 2680 Woodlawn Drive, Honolulu, Hawaii 96822, USA ¹²Physics Department2320 Chamberlin Hall, University of Wisconsin-Madison, 1150 University Avenue Madisol Visconsin 53706-1390 USA ¹³Department ofAstronomy and AstrophysicЫniversity ofChicago,Chicago,Illinois 60637,USA ^{l4}Kavli Institute for Cosmological Physic**s**Jniversity ofChicago,Chicago,Illinois 60637,USA ¹⁵Departmentof Physics and AstronomyUniversity of Pennsylvania. Philadelphia, Pennsylvania 19104USA ¹⁶CNRS,UMR 7095, Institut d'Astrophysique de ParisF-75014 Paris, France ¹⁷Sorbonne Universitá, UPMC Univ Paris 06, UMR 7095, Institut d'Astrophysique de Paris, F-75014 Paris.France ¹⁸Department ofPhysics,Northeastern UniversityBoston,Massachusetts 02115JSA

```
<sup>19</sup>High-Energy Physics DivisionArgonne NationalLaboratory,
                       9700 South Cass Avenuergonne, Illinois 60439, USA
            <sup>20</sup>University ObservatoryFaculty of Physics,Ludwig-Maximilians-Universität,
                               Scheinerstr.1, 81679 Munich, Germany
                <sup>21</sup>Department of Physics and AstronomyUniversity College London,
                         Gower StreetLondon WC1E 6BTUnited Kingdom
   <sup>22</sup>Kavli Institute for Particle Astrophysics and Cosmology, O. Box 2450, Stanford University,
                                   Stanford, California 94305, USA
            <sup>23</sup>SLAC NationalAccelerator Laboratory, Menlo Park, California 94025, USA
           <sup>24</sup>Instituto de Física Teórica Universidade Estadua Paulista, São Paulo, Brazil
     <sup>25</sup>Department of Physics, Carnegie Mellon University Pittsburgh, Pennsylvania 15312 JSA
<sup>26</sup>Enrico Fermi Institute, University of Chicago, 5640 South Ellis Avenue, Chicago, Illinois, 60637, USA
<sup>27</sup>Department of Physics, University of Chicago, 5640 South Ellis Avenue, Chicago, Illinois 60637, USA
              <sup>28</sup>Instituto de Astrofisica de Canaria<del>⊊</del>-38205 La Laguna,Tenerife,Spain
     <sup>29</sup>Universidad de La LagunaDepartmento Astrofísicæ-38206 La Laguna,Tenerife,Spain
        <sup>30</sup>Center for AstrophysicaSurveysNational Center for Supercomputing Applications.
                        1205 WestClark Street, Urbana, Illinois 61801, USA
              <sup>31</sup>Department ofAstronomy,University of Illinois at Urbana-Champaign,
                         1002 W. Green Street Urbana, Illinois 61801, USA
   <sup>32</sup>Institut de Física d'Altes Energies (IFAE)The Barcelona Institute oScience and Technology,
                         Campus UAB 08193 Bellaterra (Barcelona) Spain
               <sup>33</sup>Physics Department/Villiam JewellCollege,Liberty, Missouri, 64068
           <sup>34</sup>Department of Physics, Duke University Durham North Carolina 27708, USA
                 <sup>5</sup>California Institute of Technology,1200 EastCalifornia Boulevard,
                           MC 249-17, Pasadena California 91125, USA
             <sup>36</sup>Departmentof Physics and Astronomy, he University of Western Ontario,
                                 London Ontario N6A 3K7, Canada
           <sup>37</sup>Institute for Earth and Space Exploration, the University of Western Ontario,
                                 London, Ontario N6A 3K7, Canada
<sup>38</sup>Jodrell Bank Center for Astrophysicsachoolof Physics and AstronomyUniversity of Manchester,
                        Oxford Road, Manchester M13 9PLUnited Kingdom
<sup>39</sup>University of NottinghamSchool of Physics and AstronomNottingham NG7 2RDUnited Kingdom
<sup>40</sup>Astronomy Unit, Department of Physics, University of Trieste, via Tiepolo 11, I-34131 Trieste, Italy
       <sup>11</sup>INAF-Osservatorio Astronomico dirieste, via G. B. Tiepolo 11, I-34143 Trieste, Italy
        <sup>42</sup>Institute for FundamentaPhysics of the Universe, Via Beirut 2, 34014 Trieste, Italy
<sup>43</sup>California Institute of Technology, 1200 East California Boulevard, Pasadena, California 91125, USA
             44Institut d'Estudis Espacials de Catalunya (IEEQ)8034 BarcelonaSpain
          <sup>45</sup>Institute of Space Sciences (ICESIC), Campus UAB, Carrer de Can Magrans,
                                     s/n, 08193 BarcelonaSpain
   <sup>46</sup>Schoolof Mathematics and Physics Iniversity of Queensland Brisbane QLD 4072 Australia
    47High Energy Accelerator Research Organization (KEK)sukuba,lbaraki 305-0801,Japan
          Department ofPhysics,University of California, Berkeley,California 94720,USA
<sup>49</sup>Centro de Investigaciones Enœticas, Medioambientales y Tecnológicas (CIEMA™) adrid, Spain
    Lawrence Berkeley National aboratory, 1 Cyclotron Road, Berkeley, California 94720, USA
              <sup>51</sup>Departmentof Physics,IIT Hyderabad,Kandi, Telangana 502285India
               <sup>52</sup>Departmentof Physics and McGillSpace InstituteMcGill University,
                      3600 Rue UniversityMontreal, Quebec H3A 2T8Canada
            <sup>53</sup>Canadian Institute for Advanced Resear®I,FAR Program in Gravity and
                     the Extreme Universe, Toronto, Ontario M5G 1Z8, Canada
         <sup>54</sup>NSF AI Planning Institute for Physics of Future, Carnegie Mellon University,
                                Pittsburgh, Pennsylvania 15213 USA
             55Université Grenoble AlpesCNRS,LPSC-IN2P3,38000 Grenoble France
               <sup>56</sup>Department of Astronomy/Steward Observator University of Arizona,
                    933 North Cherry AvenueTucson, Arizona 85721-0065USA
                   <sup>57</sup>Jet Propulsion Laboratory California Institute of Technology,
                      4800 Oak Grove Drive Pasadena California 91109, USA
           <sup>58</sup>Center for Cosmology and Astro-Particle Physion, Ohio State University,
                                    Columbus, Ohio 43210, USA
          <sup>59</sup>Departmentof Physics, The Ohio State University Columbus, Ohio 43210, USA
```

```
<sup>60</sup>Departmentof Astrophysicaland Planetary Sciences Iniversity of Colorado,
                                  Boulder, Colorado 80309, USA
                   <sup>61</sup>Department ofAstronomy,University ofCalifornia, Berkeley,
                        501 CampbellHall, Berkeley, California 94720, USA
                     <sup>62</sup>Institute of Theoretical Astrophysics University of Oslo.
                          P.O. Box 1029 Blindern, NO-0315 Oslo, Norway
     <sup>63</sup>European Southern Observatorkarl-Schwarzschild-Straße 2,5748 Garching,Germany
     <sup>64</sup>Observatório NacionalRua Gal. José Cristino 77, Rio de Janeiro, RJ-20921-400 Brazil
          65Departmentof Physics, University of Colorado, Boulder, Colorado 80309, USA
              <sup>66</sup>Departmentof Physics,University ofOxford, Denys Wilkinson Building,
                          Keble Road, Oxford OX1 3RH, United Kingdom
 <sup>67</sup>Schoolof Physics and AstronomyCardiff University, Cardiff, Wales CF24 3AA,United Kingdom
                <sup>58</sup>Department of Astronomy University of Illinois Urbana-Champaign,
                       1002 WestGreen Street Urbana, Illinois 61801, USA
                 <sup>69</sup>Departmentof Physics,University of Illinois Urbana-Champaign,
                       1110 WestGreen StreetUrbana, Illinois 61801, USA
            <sup>70</sup>Canadian Institute for Advanced Researta, FAR Program in Gravity and
                     the Extreme Universe Toronto, Ontario M5G 1Z8, Canada
           <sup>71</sup>Santa Cruz Institute for Particle Physicsanta Cruz, California 95064, USA
          <sup>72</sup>University of Chicago, 5640 South Ellis Avenu@hicago, Illinois 60637, USA
               <sup>3</sup>Department ofPhysics,University ofArizona, Tucson AZ 85721USA
                          <sup>74</sup>Harvard-Smithsonian Center for Astrophysics,
                     60 Garden StreetCambridge, Massachusetts 0213&ISA
<sup>75</sup>Departmentof Physics, University of California, One Shields Avenu@avis, California 95616, USA
      <sup>76</sup>Australian Astronomical OpticsMacquarie UniversityNorth Ryde NSW 2113Australia
             <sup>77</sup>Lowell Observatory,1400 Mars Hill Road,Flagstaff,Arizona 86001,USA
    <sup>78</sup>Physics DivisionLawrence Berkeley Nationalaboratory, Berkeley, California 94720, USA
          <sup>79</sup>Department of Physics and Astronom Pevensey Buildind University of Sussex.
                                Brighton BN1 9QH, United Kingdom
               80 Instituto de Astrofísica e Ciências do Espaçoaculdade de Ciências,
                        Universidade de Lisboal 769-016 Lisboa Portugal
                     <sup>81</sup>Centre for Gravitational AstrophysicsCollege ofScience,
                   The Australian NationaUniversity, Acton ACT 2601 Australia
       <sup>82</sup>The Research Schoolf Astronomy and Astrophysic Australian National University,
                                    Acton ACT 2601 Australia
      83Departmentof Applied Mathematics and Theoretic hysics, University of Cambridge,
                              Cambridge CB3 0WAUnited Kingdom
  <sup>84</sup>George P.and Cynthia Woods Mitchellnstitute for Fundamental Physics and Astronomand
 Department of Physics and Astronom Texas A&M University College Station Texas 77843USA
        85Department of Astronomy, The Ohio State University Columbus, Ohio 43210, USA
<sup>86</sup>Radcliffe Institute for Advanced StudMarvard University, Cambridge, Massachusetts 0213&ISA
                    <sup>87</sup>Departmentof AstrophysicalSciencesPrinceton University,
                          Peyton Hall, Princeton, New Jersey 08544USA
           88 Institució Catalana de Recerca i Estudis Avança Es 08010 Barcelona Spain
           89Excellence Cluster Univers & oltzmannstraße 28,5748 Garching, Germany
 90Max Planck Institute for ExtraterrestriaPhysics, Giessenbachstrass $5,748 Garching, Germany
                Perimeter Institute for TheoreticaPhysics,31 Caroline StreetNorth,
                                Waterloo, Ontario N2L 2Y5, Canada
<sup>92</sup>Department ofPhysics,Stanford University,382 Via Pueblo Mall,Stanford,California 94305,USA
               <sup>93</sup>Dunlap Institute for Astronomy & Astrophysics Iniversity of Toronto,
                     50 St. George Street, Toronto, Ontario M5S 3H4, Canada
             <sup>94</sup>Instituto de Física Gleb Wataghir Universidade Estadual de Campinas,
                                  13083-859 CampinasSP, Brazil
             95Departmentof Physics, University of Surrey, Guildford, United Kingdom
          <sup>96</sup>Kavli Institute for the Physics and Mathematics to Universe (WPI) UTIAS,
                     The University of Tokyo, Kashiwa, Chiba 277-8583, Japan
  <sup>97</sup>Hamburger SternwarteUniversitätHamburg,Gojenbergsweg 1122,1029 Hamburg,Germany
                    <sup>98</sup>Schoolof Physics and AstronomyUniversity ofMinnesota,
                     116 Church StreeSE MinneapolisMinnesota 55455USA
```

of gravitational lensing. Although CMB photons originate

(Received 27 June 2022; accepted 15 November 2022b) lished 31 January 2023)

We present cosmological constraints from the analysis of two-point correlation functions between galaxy positions and galaxy lensing measured in Dark Energy Survey (DES) Year 3 data and measurements of cosmic microwave background (CMB) lensing from the South Pole Telescope (SPT) and Planck. When jointly analyzing the DES-only two-point functions and the DES cross-correlations with SPT b Planck CMB lensing, we find Ω ½ 0.344 0.030 and $S_s \equiv \sigma_8 \delta \Omega_m = 0.3 \beta^5 \% 0.773 0.016$, assuming Λ CDM. When additionally combining with measurements of the CMB lensing autospectrum, we find $\Omega_{\,\mathrm{m}}$ 1/4 $0.30_{-0.021}^{+0.018}$ and S₈ 1/4 0.792 0.012. The high signal-to-noise of the CMB lensing cross-correlations enables several powerful consistency tests of these results, including comparisons with constraints derived from cross-correlations onlyand comparisons designed to test the robustness of the galaxy lensing and clustering measurements from DESpplying these tests to our measurements, find no evidence of significant biases in the baseline cosmological constraints from the DES-only analyses or from the joint analyses with CMB lensing cross-correlations However, the CMB lensing cross-correlations suggest possible problems with the correlation function measurements using alternative lens galaxy samples, particular the REDMAGIC galaxies and high-redshifMAGLIM galaxies, consistent with the findings of previous studies. We use the CMB lensing cross-correlations to identify directions for further investigating these problems.

DOI: 10.1103/PhysRevD.107.023531

I. INTRODUCTION

from the last scattering surface atedshift z ~ 1100, their The late-time large scale structure (LSS) of the University paths are perturbed by structure at late times, including the is sensitive to a variety of cosmologicasignals, ranging same LSS measured by galaxy surveys. CMB lensing from the properties of dark energy and dark matter, to the provides a highly complementary probe of structure to masses of the neutrinos. Galaxy imaging surveys probe this galaxy surveys, and cross-correlation between the two structure using observations of both the positions of have severalappealing featuresFor one, current galaxy galaxies (which trace the LSS) and the shapes of galaxies maging surveys (like DES) identify galaxies out to $z \sim 1$, (which are distorted by the gravitational lensing effects of but the galaxy lensing measurements with these surveys do the LSS). Several galaxy imaging surveys have used two not have significants ensitivity beyond $z \approx 0.75$ Without point correlations between these measurements to place the high-redshift lensing information, cosmological conconstraints on cosmological models, including the Kilo straints from galaxy surveys at $z \ge 0.75$ are therefore Degree Survey (KiDS),the Hyper Suprime Cam Subaru significantly degraded.CMB lensing, however, reaches Strategic Program (HSC-SSP), and the Dark Energy Surveyak sensitivity at z ~ 2. Therefore, by cross-correlating (DES) [e.g., 1–3]. DES has recently presented cosmologigalaxy surveys with CMB lensing measurements, it is cal constraints from the joint analysis of the three two-pointossible to obtain high-precision measurements of the correlation functions (3 × 2 pt) between measurements of evolution of the matter distribution over a broader range these probes from the first three years (Y3) of DES data [4]. redshifts than by using galaxy surveys alone Cross-

Surveys of the cosmic microwave background (CMB) correlations of galaxy surveys with CMB lensing meaare also able to probe the late-time LSS through the effects rements are also expected to be robust to certain types of systematic biasesBecause the galaxy survey measure-(e.g., they use data measured by differentelescopes at correlate with biases in CMB lensing, making two-point functions between the two especially robust. Finally, crossare minimally correlated with the 5 × 2 ptmeasurements encies than correlations within a survey, offering the possibility of improved parameterconstraints via degeneracy breaking in joint analyses.

The prospect of obtaining tighter and more robust cosmologicalconstraints from the late-time matter distribution via cross-correlations is particularly timely given recent hints of tensions between some cosmological probenerefore also analyze various subsetsof the 6 × 2 pt In particular, recent observations of late-time structure from galaxymistenditemprefer lower values of $S_8 \equiv \sigma_8$ $\Omega_m = 0.3$ than CMB surveys [5–9]. This tension could result from physics beyond the standard cosmologi-DES Y3 data of discrepancies in the galaxy bias values cal constant and cold dark matter model (ΛCDM), or it could result from systematic biases in the analysesBy cross-correlating galaxy surveys with CMB lensing,we obtain an independent andle on the late-time large scale structure measurements that can be used to investigate the smological results presented in [4]. Surprisingly, the origins of this possible tension [10–13] Recentanalyses have also suggested the possibility of systematic biases in galaxy survey measurements 14]. Because crosscorrelations between galaxy surveysand CMB lensing are robustto many important sources of systematic error, There is no known physical explanation for this discrepthey provide a powerful way to ensure that late-time measurements of structure are unbiased.

This work presents the joint cosmological analysis of lensing measured in DES data and CMB lensing measurements from the South Pole Telescope [SPT, 15] and the als of the present analysis. Planck satellite [16]. As part of its 2008-2011 SPT-SZ maps of the CMB that partially overlap with the full DES footprint [17]. At somewhatlower sensitivity and resolution, Planck has obtained full-sky maps of the CMB that overlap completely with the DES footprint. Together, theseoughly a factor of three larger area. Second, the CMB CMB maps enable high signal-to-noise estimation of the CMB lensing signal across the entire DES footprint [17,18], presenting an opportunity for cross-correlation studies.

From the measurements of galaxy positions (used to compute the galaxy overdensitδ_α), galaxy lensing (γ,or yt for the tangential shear), and CMB lensing (MB), it is possible to form six two-point functions: galaxy clustering us to remove a significant fraction of the small-scale $(hδ_iδ_ni)$, galaxy-galaxy lensing (hδ), cosmic shear (hγγi), galaxy density-CMB lensing cross-correlation (lh@MBi), galaxy shear-CMB lensing cross-correlation (h) and the CMB lensing auto-correlation (hus KCMBi). All six of the above will be considered here (hereafter, we refer to thism the tSZ effect allows us to extract signal from a combination as 6 × 2 pt). The five two-point functions

excluding the CMB lensing autocorrelation (referred to as ments are so different from the CMB lensing measurements 2 pt) all probe structure below about at z ≤ 1.25, and are highly correlated. This combination, which we measure different wavelengthsand use different estimators for the using DES, SPT, and Planck data is the primary focus of lensing signal), biases in the galaxy surveys are unlikely this work. The CMB lensing autocorrelation measurements used in this analysis are derived from all-sky Planck data, and survey correlations often have different parameter dependwing to their small (fractional) sky overlap and sensitivity to higher redshifts [18]. We therefore treathe CMB lensing autocorrelation as an externarobe, and combine it with 5 × 2 pt at the likelihood level.

As highlighted above, one of the key reasons to consider cross-correlations of galaxy surveys with CMB lensing is to improve robustness to systematic uncertaintie we will probes for the purposes of testing robustness and exploring sensitivity to possible systematic errors. Of particular interest for these tests is the unexpected discovery in preferred by the clustering and lensing measurements. The DES Y3 analysis considered two galaxy samples for the purposes of measuring: MAGLIM and REDMAGIC. The MAGLIM galaxies at $z \le 0.8$ were used for the baseline galaxy bias values inferred for EDMAGIC galaxies from their clustering were found to be roughly 10% lower than the bias values inferred from lensing [19], with this discrepancy increasing forthe highest-redshiftgalaxies. ancy, but tests in [19] suggest that it may be connected to observational systematics imparting additional clustering power. MAGLIM galaxies at high redshift ($z \ge 0.8$) also two-point correlations between galaxy positions and galaxyhowed a discrepancy between clustering and lensing [20]. Further investigating these discrepancies is one of the main

The analysis presented here makes seversignificant survey, SPT obtained high-resolution and high-sensitivity improvements relative to previous cross-correlation analyses between DES and SPT/Planck measurements of CMB lensing [21–27]. First, the DES data have significantly expanded in going from Y1 observations to Y&overing lensing maps from SPT/Planck have been remade with severalimprovements (described in more detail [18]). Foremostamong these is that we have used the CMB lensing estimator from [28] to reduce contamination in the lensing maps from the thermaSunyaev-Zel'dovich (tSZ) effect. This contamination wasthe dominant source of systematic uncertainty for the analysis of [27], and required measurements from our analysis to ensure that our results were unbiased. As a result, the total signal-to-noise of the CMB lensing cross-correlations was significantly reduced. Using a CMB lensing map that is immune to contamination wider range of angular scales and hence improve our

signal-to-noise ratio. Finally, we have also implemented severalimprovements to the modeling of the correlation functions, which are described in more detail in [18].

The analysis presented here is the last in a series of three papers:In [18, hereafterPaperI] we described the construction of the combined, tSZ-cleaned SPT b Planck CMB lensing map and the methodology of the cosmological analysis. In [12, hereafter Paper II], we presented the measurements of the cross-correlation probes $h\delta_t \kappa_{CMB}i \not = h\gamma_t \kappa_{CMB}i$, a series of diagnostic tests of the measurements and cosmological constraints from this cross-correlation combination this paper (Paper III), we present the joint cosmological constraints from all the 6 × 2 pt probes, and tests of consistency between various combinations of two-point functions.

The plan of the paper is as follows. In Sec. II we describe the datasets from DES, SPT and Planck that we use in this analysis, and in Sec. III we provide an abridged summary of our model for the correlation function measurements. In Sec. IV, we present cosmological constraints from the joint analysis of cross-correlationsbetween DES and CMB lensing measurements from SPT and Planakad discuss by the cross-correlationmeasurements. We conclude in Sec. V.

II. DATA FROM DES, SPT AND PLANCK

DES [29] is a photometric survey in five broadband filters (grizY), with a footprint of nearly 5000 degof the southern sky, imaging hundreds of millions of galaxies. It employs the 570-megapixel Dark Energy Camera [DECam, 30] on the Cerro Tololo Inter-American Observatory (CTIO) 4 m Blanco telescope in ChileWe use data from the first three years (Y3) of DES observations. The foundation of the various DES Y3 data products is the Y3 Gold catalog described in [31], which achieves a deptlCMB lensing maps cover the full DES Y3 survey region. of S=N ~ 10 for extended objects up to i ~ 23.0 over an types of galaxy samples:lens galaxies that are used as biased tracers of the underlying density fieldand source galaxies which are used to measure the shape-distorting these two patches inding good agreement. effects of gravitationallensing. We use the same galaxy samples as in the DES 3 × 2 panalysis [4]. That is, the lens galaxies are taken from the four-redshift binaGLIM taken from the four-redshift bimetacalibration sample described in [33]. We will additionally consider lens galaxies from the REDMAGIC sample described in [19]. In particular, we will investigate the potentia systematic biases that led to that sample not being used as the baselimour esponding constraints at the likelihood level; this cosmology sample in [4]. The redshift distributions for the approximation is validated in Paper I. MAGLIM, REDMAGIC, METACALIBRATION samples are

shown in Fig. 1. As mentioned above, we use two CMB lensing maps indark matter model, and a cosmological model where the this work: one covering the SPT-SZ footprint that uses dataquation of state parameter of dark energy, w, is

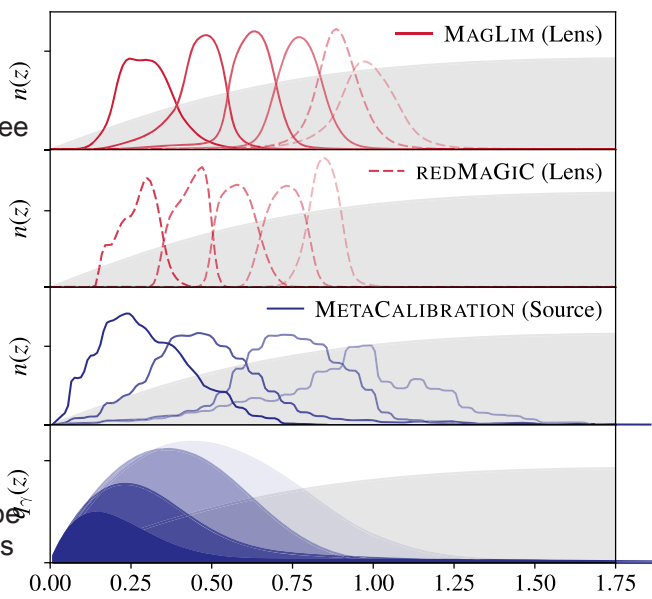


FIG. 1. Redshift distributions of the galaxy samples considered in this work. The MAGLIM (top panel) and REDMAGIC (second several tests of the robustness of these constraints enabled to measure the galaxy overdensity, while the etacalibration (third from top) source galaxy samples are used to measure weak lensin@ur main cosmological results use only the first four bins of threaglim sample (solid lines). We perform tests with alternate samples (dashed lines) for exploratory and diagnostic purposes the bottom panel we show the lensing kernels [Eq. (3)] corresponding to the source galaxies (blue). The gray band in every panel represents the CMB lensing kern (4)].

from SPT-SZ and Planck (with an overlapping area of ~1800 deg), and a second that covers the northern part of the DES survey that uses only Planck data (with an overlapping area of ~2200 deg). Together, these two Since the noise levels and beam sizes of SPT-SZ and unmasked area of 4143 detn this work, we consider two Planck are different, the resulting CMB lensing maps must be treated separately in our analysis. In Paper II we tested the consistency between the cosmological constraints from

III. MODELING AND MEASUREMENTS

sample described in [32], and the source galaxy shapes are The theoretical framework we use in this analysis is laid out in Paper I and [34]. The full 6 × 2 pt data vector consists of six two-point functions. Since there is little correlation between 5 × 2 pand the CMB lensing autocorrelation measurements from Planckye combine the

> We fit the 6 × 2 pt data to two different cosmological models: a spatially flat, cosmologicalconstantand cold

additionally allowed to vary. Following the DES convention, we will refer to these models as ACDM and wCDM; Paper I and [34] for details. note, though, that we allow the sum of the neutrino masses (i) Galaxy bias: Our baseline model assumed inear to vary in both of these analyses.

The modeling of the 5×2 pt correlations begins with the auto and cross-power spectrum of the three fields, (δ_1) κ_{CMB}). For the correlation functions other than galaxy clustering, we use the Limber approximation [35]:

$$C^{X^iY^j} \tilde{\delta} l P^{1/4} = d\chi \frac{q_X^i \tilde{\delta} \chi P_X^j \tilde{\delta} \chi P}{\chi^2} P_{NL} = \frac{l \not p \ 1=2}{\chi}; \ z \tilde{\delta} \chi P; \quad \tilde{\delta} 1 P_{NL} = \frac{l \not p \ 1=2}{\chi}; \ z \tilde{\delta} \chi P; \quad \tilde{\delta} 1 P_{NL} = \frac{l \not p \ 1=2}{\chi}; \ z \tilde{\delta} \chi P; \quad \tilde{\delta} 1 P_{NL} = \frac{l \not p \ 1=2}{\chi}; \ z \tilde{\delta} \chi P; \quad \tilde{\delta} 1 P_{NL} = \frac{l \not p \ 1=2}{\chi}; \ z \tilde{\delta} \chi P; \quad \tilde{\delta} 1 P_{NL} = \frac{l \not p \ 1=2}{\chi}; \ z \tilde{\delta} \chi P; \quad \tilde{\delta} 1 P_{NL} = \frac{l \not p \ 1=2}{\chi}; \ z \tilde{\delta} \chi P; \quad \tilde{\delta} 1 P_{NL} = \frac{l \not p \ 1=2}{\chi}; \ z \tilde{\delta} \chi P; \quad \tilde{\delta} 1 P_{NL} = \frac{l \not p \ 1=2}{\chi}; \ z \tilde{\delta} \chi P; \quad \tilde{\delta} 1 P_{NL} = \frac{l \not p \ 1=2}{\chi}; \ z \tilde{\delta} \chi P; \quad \tilde{\delta} 1 P_{NL} = \frac{l \not p \ 1=2}{\chi}; \ z \tilde{\delta} \chi P; \quad \tilde{\delta} 1 P_{NL} = \frac{l \not p \ 1=2}{\chi}; \ z \tilde{\delta} \chi P; \quad \tilde{\delta} 1 P_{NL} = \frac{l \not p \ 1=2}{\chi}; \ z \tilde{\delta} \chi P; \quad \tilde{\delta} 1 P_{NL} = \frac{l \not p \ 1=2}{\chi}; \ z \tilde{\delta} \chi P; \quad \tilde{\delta} 1 P_{NL} = \frac{l \not p \ 1=2}{\chi}; \ z \tilde{\delta} \chi P; \quad \tilde{\delta} 1 P_{NL} = \frac{l \not p \ 1=2}{\chi}; \ z \tilde{\delta} \chi P; \quad \tilde{\delta} 1 P_{NL} = \frac{l \not p \ 1=2}{\chi}; \ z \tilde{\delta} \chi P; \quad \tilde{\delta} 1 P_{NL} = \frac{l \not p \ 1=2}{\chi}; \ z \tilde{\delta} \chi P; \quad \tilde{\delta} 1 P_{NL} = \frac{l \not p \ 1=2}{\chi}; \ z \tilde{\delta} \chi P; \quad \tilde{\delta} 1 P_{NL} = \frac{l \not p \ 1=2}{\chi}; \ z \tilde{\delta} \chi P; \quad \tilde{\delta} 1 P_{NL} = \frac{l \not p \ 1=2}{\chi}; \ z \tilde{\delta} \chi P; \quad \tilde{\delta} 1 P_{NL} = \frac{l \not p \ 1=2}{\chi}; \ z \tilde{\delta} \chi P; \quad \tilde{\delta} 1 P_{NL} = \frac{l \not p \ 1=2}{\chi}; \ z \tilde{\delta} \chi P; \quad \tilde{\delta} 1 P_{NL} = \frac{l \not p \ 1=2}{\chi}; \ z \tilde{\delta} \chi P; \quad \tilde{\delta} 1 P_{NL} = \frac{l \not p \ 1=2}{\chi}; \ z \tilde{\delta} \chi P; \quad \tilde{\delta} 1 P_{NL} = \frac{l \not p \ 1=2}{\chi}; \ z \tilde{\delta} \chi P; \quad \tilde{\delta} 1 P_{NL} = \frac{l \not p \ 1=2}{\chi}; \ z \tilde{\delta} \chi P; \quad \tilde{\delta} 1 P_{NL} = \frac{l \not p \ 1=2}{\chi}; \ z \tilde{\delta} \chi P; \quad \tilde{\delta} 1 P_{NL} = \frac{l \not p \ 1=2}{\chi}; \ z \tilde{\delta} \chi P; \quad \tilde{\delta} 1 P_{NL} = \frac{l \not p \ 1=2}{\chi}; \ z \tilde{\delta} \chi P; \quad \tilde{\delta} 1 P_{NL} = \frac{l \not p \ 1=2}{\chi}; \ z \tilde{\delta} \chi P; \quad \tilde{\delta} 1 P_{NL} = \frac{l \not p \ 1=2}{\chi}; \ z \tilde{\delta} \chi P; \quad \tilde{\delta} 1 P_{NL} = \frac{l \not p \ 1=2}{\chi}; \ z \tilde{\delta} \chi P; \quad \tilde{\delta} 1 P_{NL} = \frac{l \not p \ 1=2}{\chi}; \ z \tilde{\delta} \chi P; \quad \tilde{\delta} 1 P_{NL} = \frac{l \not p \ 1=2}{\chi}; \ z \tilde{\delta} \chi P; \quad \tilde{\delta} 1 P_{NL} = \frac{l \not p \ 1=2}{\chi}; \ z \tilde{\delta} \chi P; \quad \tilde{\delta} 1 P_{NL} = \frac{l \not p \ 1=2}{\chi}; \ z \tilde{\delta} \chi P; \quad \tilde{\delta} 1 P_{NL} = \frac{l \not p \ 1=2}{\chi}; \ z \tilde{\delta} \chi P; \quad \tilde{\delta} 1 P_{NL} = \frac{l \not p \ 1=2}{\chi}; \ z \tilde{\delta} \chi$$

where X; $Y \in f\delta_g$; γ ; $\kappa_{CMB}g$, i, j labels the redshift bin, P_{NI} ðk; zÞ is the non-linear matter power spectrumhjch we compute using CAMB and HALOFIT [36,37], χ is the comoving distance from the observer, and zōxÞis the redshift corresponding to χ. The weighting functions, qðχÞ,describe how the differenprobes respond to largescale structure adifferent distances and are given by

$$q_{\gamma}^{i} \tilde{\delta} \chi P \stackrel{1/3}{\cancel{4}} \frac{3H_{0}^{2}\Omega_{m}}{2c^{2}} \frac{\chi}{a\tilde{\delta} \chi P} \stackrel{\infty}{\underset{\chi}{\triangleright}} d\chi^{0} n_{\gamma}^{i} \tilde{\delta} z \tilde{\delta} \chi P \stackrel{dz}{\cancel{6}} \frac{\chi^{0} - \chi}{\chi^{0}}; \quad \tilde{\delta} 3P \stackrel{dz}{\cancel{6}} \frac{\chi^{0} - \chi}{\chi^{0}$$

$$q_{\kappa_{CMB}} \delta \chi P \sqrt[1/4]{\frac{3H_0^2\Omega_m}{2c^2}} \frac{\chi}{a\delta\chi} \frac{\chi-\chi}{\chi}; \qquad \qquad \delta 4P$$

where H_0 and Ω_{m} are the Hubble constant and matter density parameters, espectively, adx b is the scale factor corresponding to comoving distance xpok; zp is galaxy bias as a function of scale (k) and redshift;-pɔzb are the normalized redshift distributions of the lens/source galaxies in bin i. x denotes the comoving distance to the CMB last scattering surface. The sufficiency of the Limber approximation for DES Y3 measurements of his and hyvi has been demonstrated in [385ince the CMB lensing crosscorrelations measure essentially the same structure with comparable signal-to-noise Limber approximation is expected to be valid for home and hakembi as well. [38] showed, however, that the Limber approximation is not sufficient for modeling galaxy clustering at DES Y3 precision. For this correlation function, the full non-

Finally, the angular-spacecorrelation functions are in [18,34]. Note that we use the full curved-sky expressions decomposing this field for the purposes of measuring when calculating the angularspace correlation functions rather the flat-sky approximations that were used in parts of decomposition, while for measuring we consider the DES Y1 analysis.

In addition to the basic modelingdescribed abovewe also consider several other physical and observational effects. We list these below but refer the readers to

- galaxy bias, but we also explore the potential improvement from using a nonlinear galaxy bias model and including smaller angular scales in our analysis, as described in [19] and Paper I.
- Intrinsic alignments (IA): We use the tidal alignment and tidal torquing [TATT, 39] model to describe the effect of galaxy intrinsic alignments. We consider an alternate IA model in Appendix C.
- (iii) Lens magnification: Gravitationallensing by foreground mass changes the observed projected number density of lens galaxies as a result of geometric dilution and modulation of galaxy flux and size. We model this effect based on measurements in simulations as described in [34,40].
- (iv) Redshift uncertainties: There are uncertainties associated with the estimation of the redshiftdistributions of the lens and the source sample, hich we model as described in [41-43]. In [44], an alternate approach to marginalizing over uncertainties in the redshift distributions was also considered, which we explore in Appendix C.
- (v) Shear calibration uncertainties We include a prescription for uncertaintiesin shear calibration as described in [4]. We estimate uncertainties in the shearmeasurements using realistic image simulations as described in [45].
- (vi) CMB map filtering: In order to suppress very smallscale noise in the CMB lensing cross-correlations, we apply filtering to the CMB lensing maps. This filtering is included in the model as described in Paper I.
- (vii) Point mass marginalization: The correlation functions at small scales are impacted by baryonic effects that are challenging to model, such as galaxy formation. This is particularly problematic for $h\delta_{\!q}\gamma_t$ i: changesin, e.g., the massesof the lens galaxies atvery small scales can impacthe largescale hδy, i because tangentialshear is a nonlocal quantity. To reduce sensitivity of our analysis to small-scale effects in ho, we therefore adopt the point mass marginalization approach of [46], which involves modifying the covariance matrix of $\sqrt[4]{6}$.

We measure the two-point angular correlation functions Limber integrals must be computed as described in [38,340] the data using the fastree-based algorithm REECORR [47] as described in [12,48–51]The shear measurements computed from the auto- and cross-spectra as described define a spin-2 field on the sky, and there are several ways two-point functions. For measuring hyvi, we use then the correlation only with tangential sheav, [52].

The covariance matrix associated with the DES-only correlation measurements estimated using the halo

model, as described in [18,53]. To account for the complexarameter difference metric. When computing the goodness estimate the covariance of the CMB lensing crosslations combined with an analytical log-normal covariance of the classical p-value computed from the statistic that estimate, as described in [18]. We ignore covariance between correlations measured with the nonoverlapping SPT b Planck and Planck-only CMB lensing mapsThe cross-covariance between the DES-only correlations and the CMB lensing cross-correlations is computed using the log-normal model, with scaling to account for the fact that the DES-only correlation measurements use the fDES

likelihood.¹ The priors imposed on the modeparameters are shown in Table II in Appendix A. The modeling and likelihood framework is built within theosmosispackage [55]. We generate parametesamplesusing the nested samplerPOLYCHORD [56].

of overlap between DES and the CMB lensing maps.

Due to uncertainties in the modeling of the correlation functions on small scales (e.gnonlinear galaxy bias and baryonic effects on the matter power spectrum), in our likelihood analysis we remove the small-scale measurements that could potentially bias our cosmologicalconstraints. The procedure of determining these "scale cuts" described in [34] and Paper I. Note that the choice of angular scales used in the analysis varies somewhat depending on whetherwe assume a linearor nonlinear galaxy bias model. We focus on the results with linear bias, but consider the results from the nonlinear bias analysis in Appendix B.

In each of the cosmological analyses performed in this work, we include a separate likelihood constructed using a set of ratios of galaxy-galaxy lensing measurements on small scales [57]. These lensing ratios are found to primarily constrain parameters describing the intrinsic alignment model and redshift biases, and are effectively independent the 5 × 2 pt data vector.

We utilize two different statistical metrics to assess the consistency of the DES and CMB-lensing cross-correlation measurements oth internally (i.e., between the different two point functions that we measure) and with other cosmologicalprobes. To assessinternal consistencywe primarily rely on the posterior predictive distribution (PPD) methods described in [58For these assessmente will quote p-values, with p < 0.01 taken as significant evidence of inconsistency. To assess external consistency, we rely on the parameter difference methods developed in [59]. For this metric, we will guote differences between parameter constraints in terms of effective σ values, corresponding to the probability values obtained from the non-Gaussian

ities of the CMB lensing noise (which is far from white), wef fit of our measurements to a particular model, we again rely on the PPD methodology, as discussed in [58]. In this case, correlations using empirical noise realizations from simu- the associated p-values can be thought of as a generalization correctly marginalizes over parameter uncertainty.

IV. COSMOLOGICAL CONSTRAINTS

A. Baseline cosmological constraints

1. Λ CDM

survey area, while the cross-correlations only use the areasWe first presentconstraints on ACDM from the joint analysis of two-point functions involving DES galaxy For the final parameter inference, we assume a Gaussiposition and lensing measurements, and measurements of CMB lensing from SPT and Planck. Following [4], all of the results in this subsection use the four redshift bin MAGLIM lens galaxy sample.

> Figure 2 shows how the constraints from the CMB lensing cross-correlations_αko_{MB}i þ hγ_tκ_{CMB}i compare to those from 3 × 2 pt. The resulting 68% credible intervals on Q_1 , Q_2 , and Q_3 computed from the marginalized 3 × 2 pt and hδ_tκ_{CMB}i þ hγ_tκ_{CMB}i posteriors are summarized in Table I. In the same table, we list the goodness of fit p-values for 3 × 2 pt and haccmbi b hytecmbi, computed Sing the PPD formalism. As noted in [4], the goodness of fit for 3 × 2 pt alone is not particularly high, but is still above our threshold of p 1/4 0.01The goodness of fit for

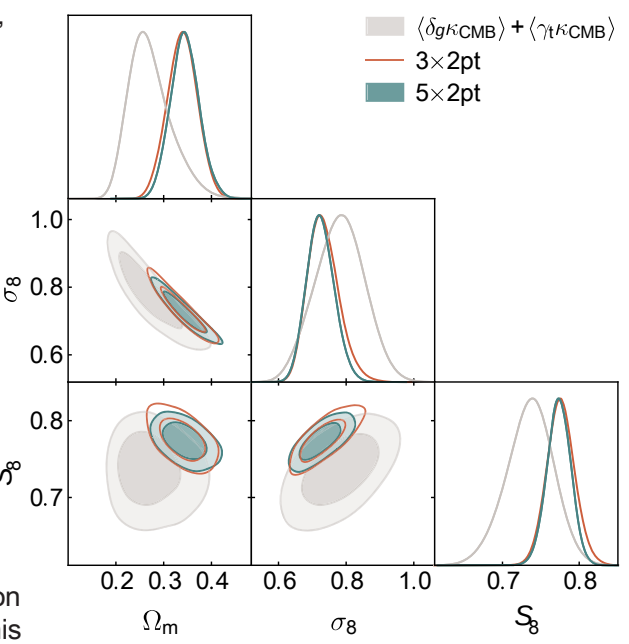


FIG. 2. ΛCDM constraints from the DES Y3 3 × 2 pt measurements (red), cross-correlations between DES Y3 galaxies and shears with SPT b Planck CMB lensing (gray), and from the joint analysis of all five two-point functions (teal). The constraints from 1See e.g., [54] for tests of the validity of this assumption in the × 2 pt are in acceptable agreement with the CMB lensing crosscorrelations, justifying the joint analysis of 5×2 pt.

context of cosmic shear, hich would also apply here.

TABLE I. Λ CDM constraints on Ω , σ_8 and $S_8 \equiv \sigma_8 \delta \Omega_m = 0.3 \, ^{6}5$ using different subsets of the 6 × 2 pt two-point functions (top five rows). The p-values correspond to the goodness of fit, as calculated using the PPD methodology. All results have use length sample and linear galaxy bias. For the 6 × 2 pt combination, we do not quote a goodness of fit because the CMB lensing autospectrum treated as an external probe. Rather, we use the parameter difference metric to assess tension between 5 × Ω by the linear galaxy. The bottom row shows constraints from Planck measurements of the primary CMB [9].

Probe	σ_8	Ω_{m}	S ₈	GoF p-value	Comments
3 × 2 pt	$0.733_{0.049}^{0.039}$	0.339 ^{0.032}	0.776 0.017	0.023	DES Collaboration etal. [4]
hδκ _{CMB} i þ hγ _t κ _{CMB} i	0.78 0.07	$0.27^{0.03}_{-0.05}$	0.74 0.03	0.50	CMB lensing cross-correlation aper II
$h\delta_{g}\gamma_{t}i \not b h\delta_{g}\kappa_{CMB}i \not b h\gamma_{t}\kappa_{CMB}i$	0.768 0.071	$0.303_{0.059}^{0.036}$	0.765 0.025	0.063	All cross-correlationsSec.IV B 2
5 × 2 pt	$0.724^{0.038}_{0.043}$	0.344 0.030	0.773 0.016	0.062	Sec.IVA
6 × 2 pt	0.785 0.029	0.306 0.018	0.792 0.012		Sec.IVA
Planck TTTEEE þ lowE	$0.793_{-0.010}^{+0.024}$	0.327@ _{0.017}	0.827 0.017		Aghanim et al.[9]

hāgkcmBi þ hytkcmBi is acceptable, as described in [12]. While the cross-correlations prefer somewhat lowerd higher σ_8 , they are statistically consistentwith 3 × 2 pt. Using the PPD formalism, we find p $\frac{1}{4}$ 0.347 when comparing the two data subsets,indicating acceptable consistencyWe are therefore justified in combining the constraints to form 5 × 2 pt, shown with the teal contours in the figure.

Given the weaker constraining power of h δ_{KCMB} i δ_{KCMB} i relative to 3 × 2 pt, the 5 × 2 pt constraints are not much tighter than the 3 × 2 pt constraints: we find an improvement of roughly 10% in the precision of the marginalized constraintson Ω_m and S_8 (see Table I). The goodness offit for the full 5 × 2 pt data vector is p $\frac{1}{4}$ 0.062, indicating an acceptable fit.

In Fig. 3 we compare the constraints from 5×2 pt with those from the CMB lensing autospectrum her k_{CMB}i. Owing to the high redshift of the CMB source plane, the CMB lensing-only contour has a different degeneracy direction than 5 × 2 pt, resulting in a weaker constraint when projecting to the Ω_m direction, but a comparable constraint in the σ_8 direction. While the CMB lensing autospectrum prefers somewhatigher σ_8 than 5 × 2 pt, the constraints are generally consistent. Because the CMB lensing autospectrum measurements are treated as an independent probe, we quantify the tension between these measurements and 5 × 2 pt using the parameter shift metric, finding a difference of 0.8 σ , indicating no evidence of significant tension. We therefore combine the two to generate constraints from allsix two-point functions, 6 × 2 pt, shown with the orange contour in the figure. Due to degeneracy breaking the joint analysis leads to notably tighter constraints on both Ω_n and σ_8 . The 1D posterior constraints on these parameters from 6 × 2 pt are summarized in Table I. Fig. 3 also shows constraints from Planck measurements of CMB temperature and polarization fluctuations [9]. We will assess consistency between our measurements and the Planck measurements in Sed.V C.

2. wCDM

We now consider constraints on wCDM, the cosmological model with a constant equation-of-state parameter of dark energy, w. The constraints from 3×2 pt, 5×2 pt, and 6×2 pt are shown in Fig. 4. We find that there is little improvement in constraining power on wCDM when adding the CMB lensing cross-correlations to 3×2 pt. Adding the h $_{\text{KMB}}$ K $_{\text{CMB}}$ i correlation, however, significantly impacts the constraints, presumably because this correlation function adds additional information about structure at

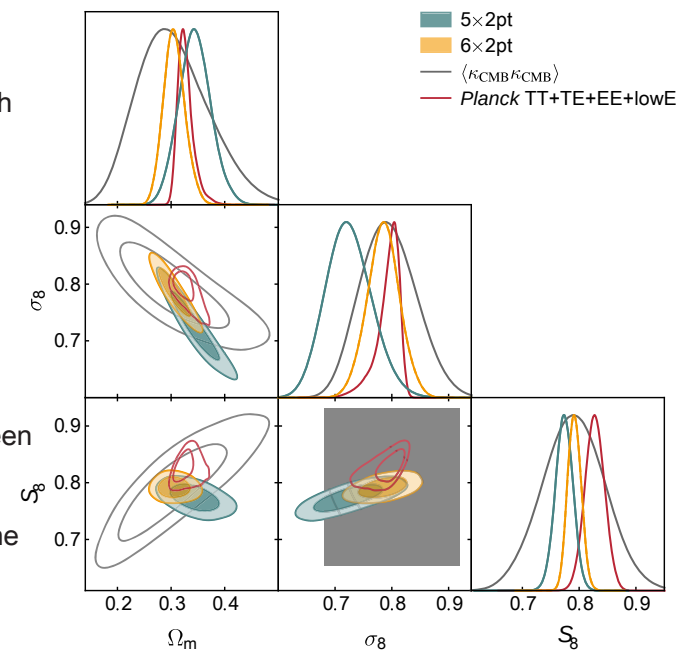


FIG. 3. ∧CDM constraints from our 5 × 2 pt analysis (teal) are compared to those from the Planck CMB lensing autospectrum measurement≰gray). The two are in acceptable agreement, justifying the joint analysis of 6 × 2 pt (orange),which yields significantly tighter constraints due to degeneracy breaking. Also shown are parameter constraints from Planck measurements of primary CMB fluctuations (TT þ TE þ EE þ lowE,dark red).

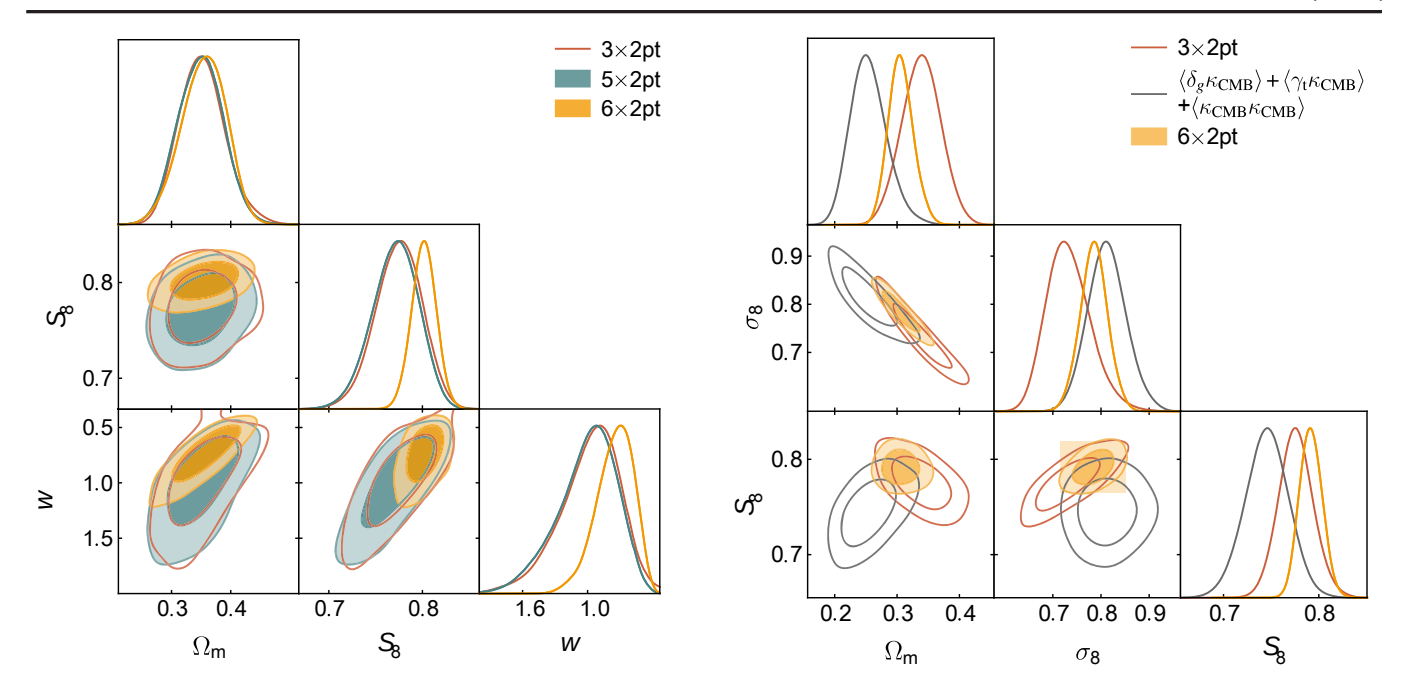


FIG. 4. Constraints on wCDM from different combinations of FIG. 5. Comparison of constraints on ΛCDM from 3 × 2 pt are essentially identicate those of 3 × 2 pt (red). Adding the CMB lensing autospectrum information in the joint 6 × 2 pt analysis (orange) significantly improves the parameterconstraints on wCDM.

z \gtrsim 1. The 6 × 2 pt analysis yields w ½ -0.7 $\[\oint_{0.14}^{0.20}$, S₈ ½ 0.801 0.013, and $\Omega_{\rm m}$ ½ 0.35 $\[\oint_{0.035}^{0.041}$. Therefore, the constraints on the dark-energy equation of state parameterare largely consistent with the cosmologicalconstant scenario of w 1/4 -1, and the constraints normal S_8 are consistent with those obtained assuming Λ CDM.

B. Robustness tests

In addition to improving cosmological constraints relative to the DES-only 3 × 2 pt analysis, a significant motivation for cross-correlating DES with CMB lensing is to test the robustness of the DES-only constraints in cross-correlations probe the same large-scale structure a $\frac{1}{3} \times 2$ pt have somewhaldifferent degeneracy directions, the DES 3 × 2 pt analysis, but with sensitivity to different potential sources of systematic bias, making them powerful cross-checks on the DES results. In this section, we subject the 6 × 2 pt data vector to several tests of internal consistency.

1.
$$3 \times 2$$
 pt vs. $\overline{3 \times 2}$ pt

We first assess the internationsistency of the 6 × 2 pt combination of probes by comparing constraints from 3 × 2 pt to the other three two-point functions making up 6 × 2 pt, which we call 3×2 pt (i.e., $h \xi_{KCMB}$ i b hγκ $_{CMB}$ i β hκ $_{CMB}$ κ $_{CMB}$ i). This comparison is shown in Fig. 5. We find that the constraining power from 3×2 pt is very similar to that of 3×2 pt. Because

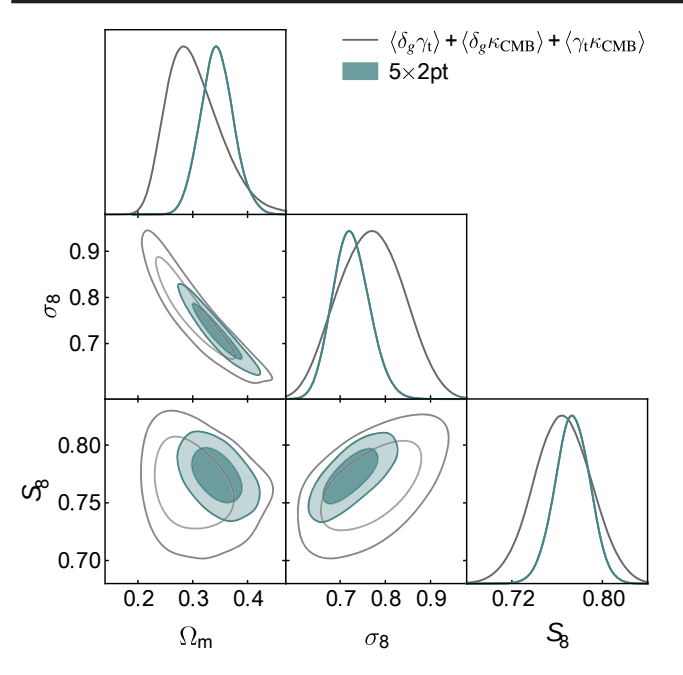
two-point functions. The 5 × 2 pt constraints (teal) on this mode(red) with the constraints from the other probes of 6 × 2 pt, i.e., $hδ_t κ_{CMB} i þ hγ_t κ_{CMB} i þ hκ_{CMB} κ_{CMB} i (gray)$. The joint analysis of both (6 × 2 pt) is shown in orangeThe two subsets of the full 6 × 2 pt analysis are in reasonable agreement. The 6 × 2 pt analysis prefers higher₈Sthan either of the two subsets.

3 × 2 pt does not constrain galaxy bias or intrinsic alignment parameters very well, applying the PPD methodology to test consistency between 3 × 2 ptand 3 × 2 pt is not well motivated. However, we note that we have already tested the consistency of x 2 pt with $h\delta_{KCMB}i$ b $h\gamma_t \kappa_{CMB}i$ (i.e., part of 3×2 pt), finding acceptable agreement (p $\frac{1}{4}$ 0.347).

Figure 5 makes it clear why 6 × 2 pt prefers a somewhat higher value of S_8 than 3×2 pt. It is not the case that 3 × 2 pt prefers a higher value of Shan 3 × 2 pt; indeed, the opposite is true Rather the slightly high value of Sa found for 6 × 2 pt is caused by the fact that 3 × 2 pt and and intersect at high value of S₈ for both probes.

2. Cross-correlations

Cross-correlationsbetween different observablesare generally expected to be more robust to systematic biases than auto-correlations of those observables ditive systematics that impact a single observable are expected to drop out of cross-correlations with another observable that has uncorrelated systematics Fig. 6 we compare the cosmological constraints obtained from only correlations to those from the full 5 × 2 pt. It is clear that removing the information from the auto-correlations particularly cosmic shear—degrades the constraints somewhat. However, we find that the value of Snferred only



2 pt (teal) to those that result from only cross-correlations betweengalaxy lensing and CMB lensing, and their crossconstraining power is lost by removing the autocorrelations. resulting constraints on Se consistent with those of the baseline analysis yields a constraint on S₈ that is in excellent analysis, providing a powerful robustness test.

from cross-correlations is consistent with that inferred from the full 5 × 2 pt analysis. This suggests that additive biases are unlikely to be having a major impact on the DES 3 × 2 pt cosmology results. Using the PPD formalism to evaluate the goodness of fit of the cross-correlations conditioned on the posterior from 5 × 2 pt, we find p ¼ 0.054, indicating an acceptable level consistency between the 5 × 2 pt constraints and the cross-correlations measurements.

3. Lensing only

The relationship between galaxy overdensity and the underlying matter field—galaxy bias—presents a significant challenge for analyses of the galaxy distribution. The baseline 3 × 2 pt results presented in [4] and the baseline cross-correlation results presented here assume a linear galaxy bias relation when modeling the galaxy field. This model is known to break down at small scales, as investigated for the DES galaxy samples in [19]. More complex bias models, such as the perturbation theorymotivated model developed in [60], are also expected to have a limited range of validity. There is therefore value in performing analyses that use only lensing information.

the REDMAGIC and high-redshift MAGLIM galaxies show evidence of systematic biases (i.e., the samples shown with dashed lines in Fig. 1). Measurements ofgalaxy-galaxy lensing with the REDMAGIC galaxies were shown to be inconsistent with clustering measurements using those galaxies [19]. This inconsistency suggests potential problem with the REDMAGIC overdensity measurements, although it is not clear whether such issues could be impacting the galaxy-galaxy lensing measurements. tering measurements or both. Similarly, galaxy-galaxy lensing and clustering measurements with the high-redshift MAGLIM galaxies were also found to be mutually inconsistent, contributing to a very poor goodness of fit to any of the cosmological models considered. For these reasons, the high-redshift MAGLIM galaxies were removed from the cosmological analysis in [4]. These issues, which we investigate further in Sec. IV B 6, further motivate a cosmologicalanalysis thatdoes not rely on galaxy overdensity measurements.

In Fig. 7, we present cosmological constraints from FIG. 6. Comparison of constraints on ACDM resulting from 5 gravitational lensing only, namely the two-point functions δ_{α} , γ and ϵ_{MB} (gray). Cross-correlations are expected to be robust rrelation. The lensing-only analysis obtains cosmological to additive systematics that impact only a single field. While some straints that are of comparable precision to those from the full 5 × 2 pt analysis. We find that the lensing-only agreement with the baseline analysis.

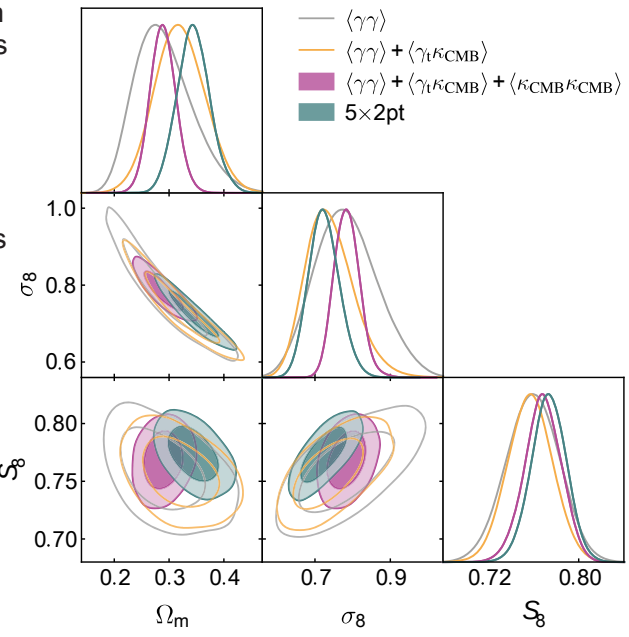
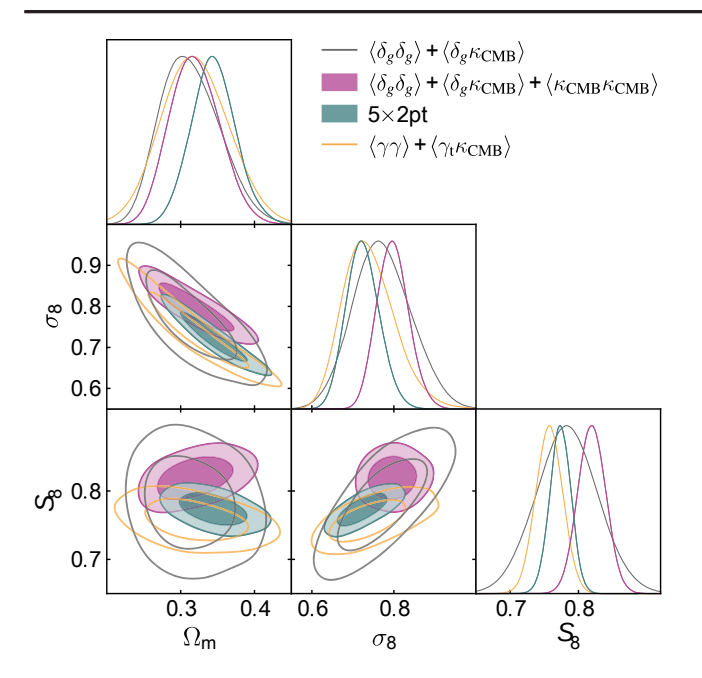


FIG. 7. Comparison of baseline 5 × 2 pt constraints on ΛCDM (teal) to constraints from various combinations of robes that only involve gravitationalensing. The lensing-only constraints are consistent with our baseline result, suggesting that any systematics which mightbe impacting the galaxy overdensity

Another motivation to consider lensing-only analyses is measurementare not dramatically biasing our cosmological that the DES galaxy overdensity measurements made witconstraints.



(teal) to constraints from those combinations of probes that do not rely on galaxy lensing (gray and purple). or reference. we also show the lensing-only constraints—excludingthe hκ_{CMB}κ_{CMB}i, which is sensitive to higher redshifts—with the orange curve.

4. No galaxy lensing

We also consider the constraints that sult from those probes that do not involve galaxy lensing. The galaxy lensing measurements ould in principle be biased by systematic errors in photometric redshifts ofthe source galaxies, shear calibration or an incorrectintrinsic alignment model. Such issues could bias constraints involving galaxy lensing, but would not impact the galaxy overdensity or CMB lensing measurements. Figure 8 shows the As $\,$ noted previously, analyses of $\,$ h $\delta_{\!_{\! q}}\delta_{\!_{\! q}}i$ $\,$ and h $\delta_{\!_{\! q}}\gamma_{\!_{\! t}}i$ constraints that result only from probes that do not include measured with the DES Y3MAGLIM [20] and REDMAGIC galaxy lensing (i.e., δ and κ_{CMB}). Again, we find that the results are consistent with those of 5 × 2 pt. Figure 8 also values of galaxy bias preferred by these two correlation shows the hγγi þ hγγ_{CMB}i constraints for comparison (i.e., lensing only, but excluding hember kcmbi, which receives contributions from higher redshifts than the other two-pointashed lines in the top panel of Figl) prefer higher bias functions). We find that the constraints involving lens galaxy overdensities are consistentith the lensing-only constraints.

Shear calibration

impacting cosmologicabonstraints from cosmic shear is biases in shearestimation [61]. Typically, estimators of lensing shearare calibrated via application to simulated lensed galaxy imagesFor the DES Year 3 cosmological analysis, calibration of shear biases is described in [45]. While this approach can be used to place tight constraintspercent) [60,65]. In [19], a new parameter, X_{lens} was on shear biases, it has the disadvantage of relying on

simulated data. A mismatch between the simulated galaxies used to calibrate the shearestimators and realgalaxies could potentially introduce systematic bias.

As pointed out in [21,62,63], joint analyses of crosscorrelations between galaxy surveysand CMB lensing measurementsoffer the potential of constraining shear calibration biases using only the data. To explore this idea, we repeatour analysis of the 3×2 pt and 5×2 pt data vectors using very wide, flat priors on the shear calibration parameters $m_i \in \tilde{o}-0.5$; 0.5 \triangleright .

The results of this analysis are shown in Fig. 9. Removing the tight priors on the insignificantly weakens the cosmological constraints from 3 × 2 pespecially the constraint on § This is because both m and impact the amplitude of the lensing correlation functionseading to strong degeneracy between the two shear calibration parameters mare also very poorly constrained without the tight priors. However, when the CMB lensing crosscorrelations are analyzed jointly with 3 × 2 pt (i.e., forming 5×2 pt), the analysis becomes significantly more robust to FIG. 8. Comparison of baseline 5×2 pt constraints on ΛCDM shear calibration. Removing the priors on weakens the cosmologicalconstraints, but not nearly as much as for 3 × 2 pt: Removing the m priors degrades the constraints on \S by a factor of 4.7 for 3 × 2 pt, but only by a factor of 2.3 for 5 × 2 pt (see rightpanel of Fig. 9). The resulting cosmological constraints are consistent ith those in the baseline analysis, providing evidence that the DES Y3 3 × 2 pt and 5 × 2 pt constraints are robust to shear calibration biases. We also find that the 5 × 2 pt data vector achieves constraints on m at roughly the 5%-10% level depending on the redshiftbin, roughly a factor of two improvement over the Y1 analysis presented in [27].

6. Investigating the X_{lens} systematic

[19] galaxy samples uncovered discrepancies between the functions. The honi measurements with AGLIM galaxies in the two highest redshift bins (i.e. those shown with the values than how i by roughly 40% to 60%. Measurements of $h \delta_{i} \delta_{\sigma} i$ with the REDMAGIC galaxies, on the other hand, show roughly 10% higher bias values than the $h\delta_{\alpha}\gamma_{t}i$ measurementsor the first four redshift bins, with this discrepancy increasing to roughly 40% for the highest A potentially significant source of systematic uncertaintyedshift bin. In principle, some difference between the bias values inferred from hδδαi and hδαγti could result from stochastic biasing [e.g., 64]. However, the amplitude of the difference seen for the REDMAGIC galaxies and the highredshift MAGLIM galaxies (roughly 10 to 40% percent) is significantly larger than expected from stochasticity (a few introduced to explore this effect:

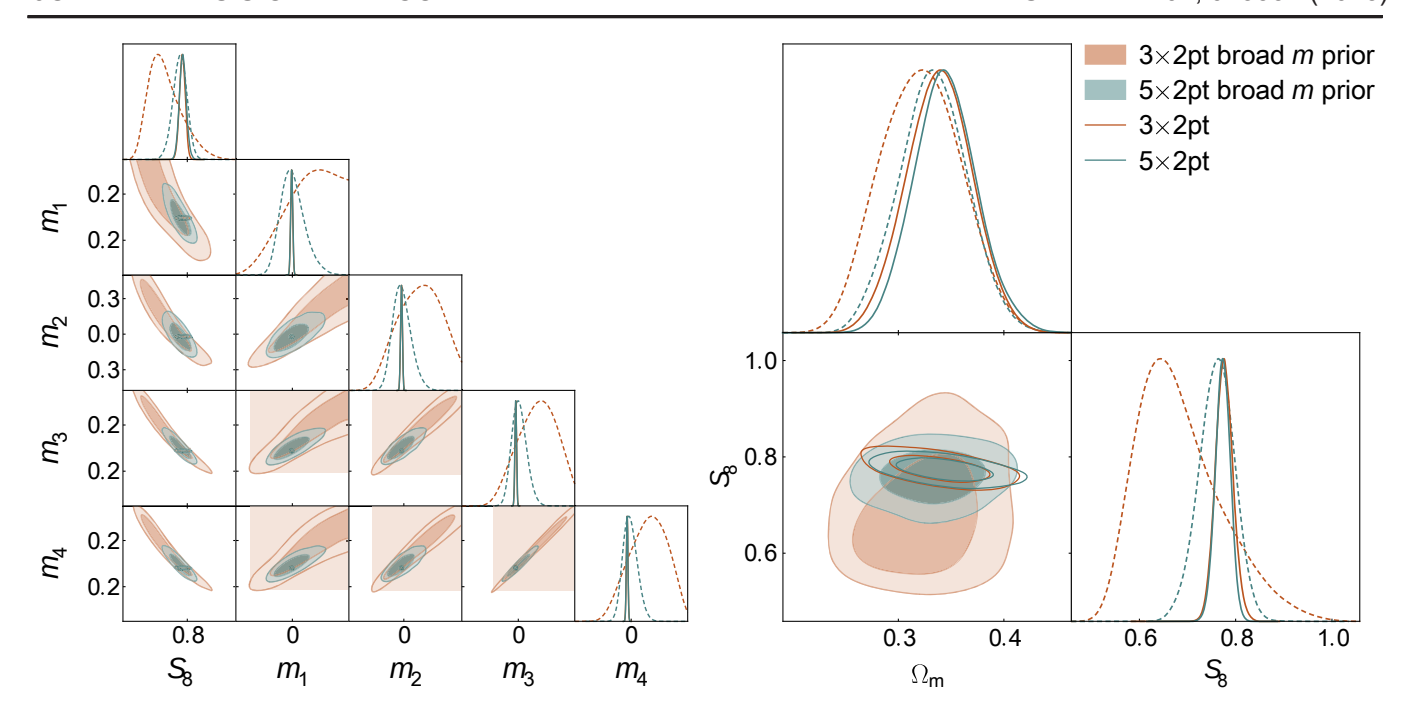


FIG. 9. Left: constraints on Sand the shear calibration parameters from 3 × 2 pt and 5 × 2 pt using different priors on With the nominal tight priors on these parameters3 × 2 pt (red dashed)and 5 × 2 pt (teal dashed)yield comparable cosmological constraints. However, when the priors grare substantially weakened, the constraints from 5 × 2 pt (teal solid) become significantly tighter than those from 3×2 pt (red solid). Similarly, the 5×2 pt analysis obtains tighter constraints **partneret**ers themselves. Right: same as left panel, but showing constraints α Right: same as left panel, but showing constraints α Right: same as left panel, but showing constraints α Right: same as left panel, but showing constraints α Right: same as left panel, but showing constraints α Right: same as left panel, but showing constraints α Right: same as left panel, but showing constraints α Right: same as left panel, but showing constraints α Right: same as left panel, but showing constraints α Right: same as left panel, but showing constraints α Right: same as left panel, but showing constraints α Right: same as left panel, but showing constraints α Right: same as left panel, but showing constraints α Right: same as left panel, but showing constraints α Right: same as left panel, but showing constraints α Right: same as left panel, but showing constraints α Right: same as left panel, but showing constraints α Right: same as left panel, but showing constraints α Right: same as left panel, but showing constraints α Right: same as left panel, but showing α Right: same as left panel, but showing constraints α Right: same as left panel, but showing α constraints from 3 × 2 ptbut has less of an impact on 5 × 2 pt.

$$X_{lens}^{i} \frac{1}{4} b_{h \xi_{i} Y_{t} i}^{i} = b_{h \xi_{i} \xi_{o} i}^{i};$$
 ð5Þ

where $b^i_{h\delta_i\gamma_t i}~(b^i_{h\delta_i\delta_h i})$ is the bias parameterfor $h\delta_g\gamma_t i$ $(h \delta_i \delta_{\sigma_i} i)$ in lens galaxy redshift bin i. The finding that of galaxy bias than the galaxy-galaxy lensing measurements amounts to a preference for X_{lens}^{i} < 1 when we expect X_{ens} ¼ 1.

The galaxy-CMB lensing cross-correlations also constrain galaxy bias, providing another handle on the anomal $\delta_{ij} \gamma_{t}$ i. As a cross-correlation, the δ_{ij} is measurements are lous values of the Kens parameter seen with the DMAGIC and high-redshiftmaglim galaxies. We show constraints on the galaxy bias parameters of the MAGLIM and REDMAGIC galaxies from three combinations of probes in Figs. 10 and 11, respectively. Each of the plotted constraints uses the combination of hyvi and his i-which are effectively independent the lens galaxies—to constrain the cosmology. The remaining probe is then chosenions at high redshifts [32]. to be $h_{Q}^{\alpha}\delta_{q}i$, $h_{Q}^{\alpha}\gamma_{t}i$, or $h_{Q}^{\alpha}\kappa_{CMB}i$, and this probe is used to constrain the galaxy bias.

For the two highest redshift bins of GLIM galaxies, we see from Fig. 10 that the δ measurements prefer higher

values of galaxy bias than the $h \xi_j \gamma_t i$ measurements, consistent with the preference for Xilens < 1 described above. Interestingly, it appears that the khone measurements prefer galaxy bias values more in line with the some of the clustering measurements prefer a higher value of the clustering measurements are considered in the clustering measurements are considered in the clustering measurements and the clustering measurements are considered in the clustering measurements. \overline{X}_{lens}^{i} < 1 is likely driven by $h\delta_{q}\gamma_{t}i$. This is perhaps not surprising, given the large residuals ofthe model fits to $h \delta_{\!\! t} \gamma_t i$ seen in [20]. However, note that there is no obvious reason for a possible failure of the baseline modeb fit expected to be guite robust to many observational systematics. Moreover, any systematic impactingwould likely show up even more strongly in to any systematic impacting y would likely show up more strongly in hyvi. Another possibility is a failure in modeling some physical effect. One such effect is lens magnification, which is known to have a significant mpact on the hδyti correla-

Fig. 11 shows the analogous bias constraints for REDMAGIC galaxies. In this case, we see that hδ_iy_ti and hδκ_{CMB}i measurementsboth prefer consistently lower values of galaxy bias than $h\delta_i\delta_{\sigma}i$, with this difference particularly pronounced in the last redshift bin. This ²This analysis is similar to that presented in [12], but differs iguggests that a possible cause of пенемасис preference $h\delta_0\delta_0$ i, it is possible that some observational systematic is

that we have allowed cosmological parameters to vary, and have $X_i^{lens} < 1$ is in the $h\delta_j \delta_g i$ measurements. In the case of data constrain the cosmologicatodel).

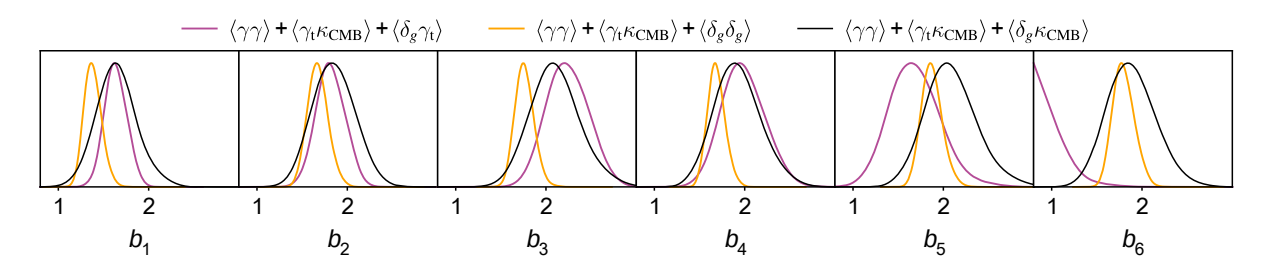


FIG. 10. Posteriors on the linear bias parameters for the AGLIM galaxies resulting from different ombinations of probesThe parameter prepresents the linear bias for the ith redshift bin. For the two highest redshift bins (excluded in the baseline cosmology analysis), galaxy clustering (ந்ந்) and galaxy-galaxy lensing (ந்ந்) prefer somewhat different values of the bias, with நிந் more in line with the values preferred by clustering.

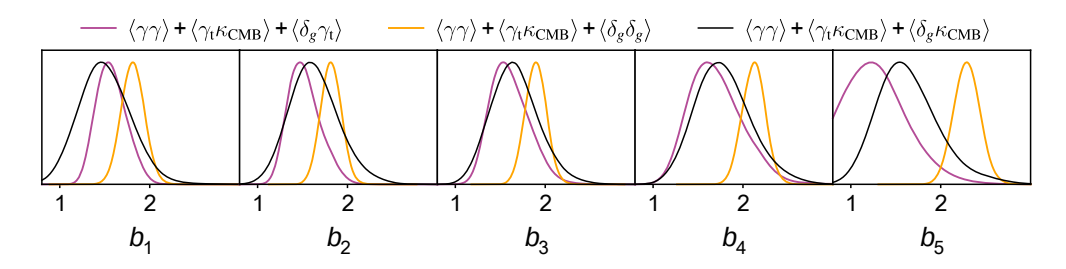


FIG. 11. Same as Fig.10, but for REDMAGIC galaxies. The bias values preferred by \$\overline{\chi_{CMB}}\$ i are in good agreement with those preferred by hδy,i, but show a preference for lower bias values than δηδαcross all redshifts.

modulating the EDMAGIC galaxy overdensity field, result- interpretation seems consiste with the observed redshift ing in a higher than expected clustering amplitude and thusends. It may be that observational systematics in δ_{α} measurements would be expected to have a less noticeable impacton $h\delta_{\!q}\gamma_t i$. At the same time,it should be emphasized that the analysis of [48] extensively tested MAGLIM from $h\delta_{\alpha}\gamma_{t}i$ at high redshift. The REDMAGIC the REDMAGIC sample for possible contamination by fore appears to be difficult to explain the anomalous X values with any known observational systematic.

The interpretation of the REDMAGIC preference for X^{lens} < 1 in terms of a systematic impactingREDMAGIC $h \delta_{\!j} \delta_{\!j} \text{i measurements is supported by tests with a modified would be consistent with mismodeling of } h \delta_{\!j} \gamma_i \text{i at high}$ REDMAGIC galaxy sample presented in [19The nominal REDMAGIC galaxy sample is selected by requiring that In [19], an alternative, "broad $\frac{2}{\lambda}$ " sample of galaxies was selected by relaxing the $\frac{1}{2}$ threshold for selection. One would expect that if an observational systematic is modulating the photometry of galaxies, it should have a smaller This is perhaps not surprising given that the systematic Indeed, it was found that for this alternate sample, the preference for $\frac{1}{4}$ ens < 1 seen for the first four redshift bins disappearsWhile it might seem surprising thathe preference for X_{lens}^{i} < 1 is possibly driven by two different factors for MAGLIM and REDMAGIC galaxies, this

a preference for higher galaxy bias. Such a systematic in the MAGIC galaxy selection are impacting the bias values inferred from $h\delta_a\delta_a$ i at low redshift, while problems in modeling haγti are impacting the bias values inferred for galaxies may be less affected by this latter systematic, various observational systematics. While some correlation they do not extend to the high redshifts probed by the last of known systematics with galaxy density is detected, thistwo redshift bins of the MAGLIM sample. We note, though, correlation is corrected using galaxy reweighting. It there-that even for REDMAGIC, the CMB lensing cross-correlations prefer higher galaxy bias than hori in the highest redshift bin; this could be suggesting that the same problem impacting the high-redshift MAGLIM galaxies is impacting the high-redshift REDMAGIC galaxies. This interpretation redshift.

The impact of the apparent systematic in the DMAGIC galaxies match a red sequence template, as measured by ample is also noticeable when the cosmological model is changed from ΛCDM to wCDM. While the DMAGIC 3 × 2 pt constraints on ACDM are quite robust to allowing the X_{lens} parameterto vary, the constraints on wCDM shift significantly when this additional freedom is introduced. impact on the broad sample than on the nominal sample biases with REDMAGIC appear to be redshift-dependent, and might therefore be somewhatlegenerate with the effects of w.

> Since our analysis above suggests thathe problems with REDMAGIC may be isolated to the clustering measurements in Fig. 12 we present constraints on wCDM

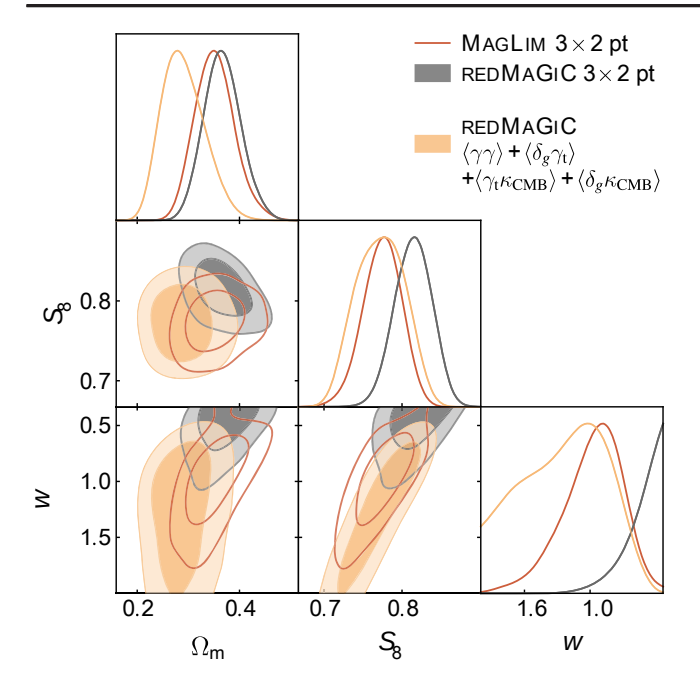


FIG. 12. Cosmological constraints on wCDM from the 3 × 2 pt data vector measured with the MAGLIM (red) and REDMAGIC (gray) lens galaxy samples. The constraints from REDMAGIC prefer surprisingly less negative w, as discussed in [4]. However constraints on Λ CDM from 5 × 2 pt and 6 × 2 pt are not when the REDMAGIC clustering measurements (1007i) are replaced by hδκ_{CMB}i þ hγ_tκ_{CMB}i to form a combination of four two-point functions (orange), the constraints agree better ith those of MAGLIM.

from the 5×2 pt combination of probes without the clustering measurementsnterestingly, we see that there is a significant shift in the constraints on w relative to the 3 × 2 pt analysis. The constraints without the clustering measurements are in good agreementith the MAGLIM

constraints. This lends additional support to the idea that the REDMAGIC clustering measurements may be systematically biased.

To summarize the above discussion analysis with CMB lensing cross-correlations suggests that there may be two different sources for the X_{lens} systematic seen with REDMAGIC and MAGLIM galaxies. For REDMAGIC galaxies, our analysis suggests apossible bias in the clustering measurements across at dshift bins. Such a bias could conceivably be caused by some observationalstematic impacting the REDMAGIC selection, which would be consistent with tests performed in [19]. At the same time, highredshift MAGLIM galaxies (and possibly high-redshift REDMAGIC galaxies as well) show evidence of a potentially different systematic error thatavors a problem with the hδ_iγ_ti fits. Such an issue could conceivably be caused by a problem with the $h\delta_h y_t$ i modeling, such as an incorrect prescription for magnification effects, which become more pronounced ahigh redshifts.

C. Consistency with Planck primary CMB measurements

As seen in Fig. 3, we find that the cosmological in significant tension with the constraints from the primary CMB measurements of Planckn particular, we compare our constraints to those from the combination of Planck TT, TE, EE, and low-IE-mode polarization measurements (Planck TT b TE b EE b lowE) [9]. Note that we do not include Planck measurements of the CMB lensing power spectrum in this combination. Using the tension metric of [59], we find that the 3×2 pt, 5×2 pt, and 6×2 pt constraints are in agreement ith Planck at the level of 1.5σ , 1.4σ , and 1.4σ , respectively. The fact that 3×2 pt

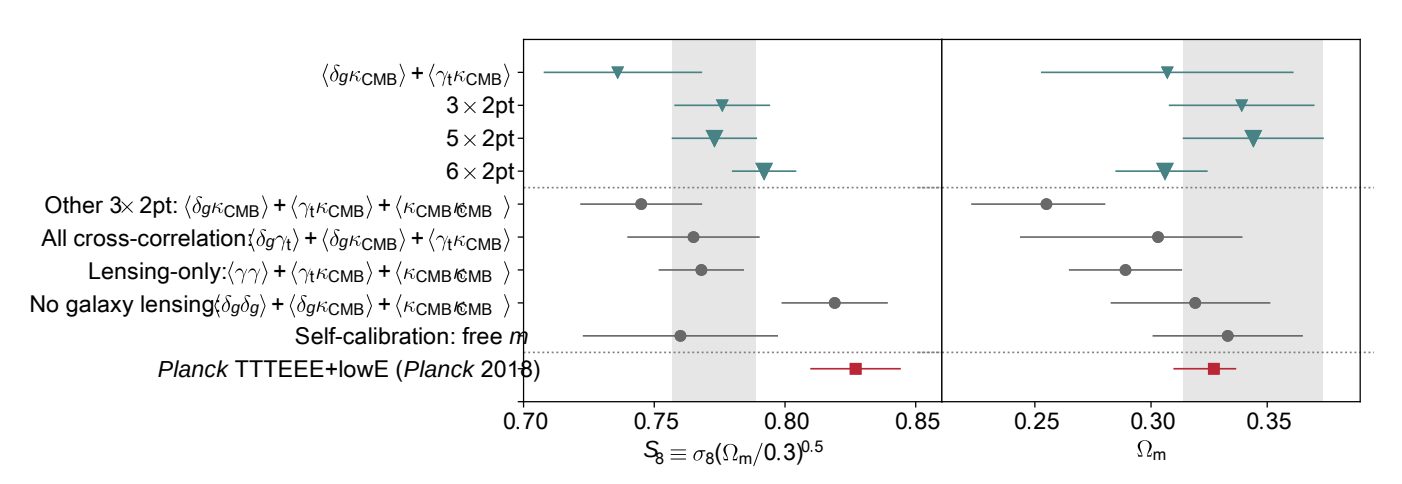


FIG. 13. Comparison of the cosmological constraints resulting from different combinations of two-point functions involving DES measurements of alaxy positions and lensing and SPT b Planck measurements of MB lensing. The gray band illustrates the constraints from 5 × 2 pt, which constitutes one of our main results; this combination of two-point functions is sensitive to structure at z ≤ 1 (unlike 6 × 2 pt, which is additionally sensitive to higher redshift structure). We also show (bottom row) constraints from Planckonly measurements of the primary CMB fluctuations. In all cases, the error bars represent 68% credible intervals determined from the marginalized posteriors on the parameters shown.

and 5 × 2 pt are roughly equally consistent with Planck is not surprising, given that the 5×2 pt constraints are guite close to those of 3×2 pt. Interestingly, while the 6×2 pt constraints are significantly tighter than 5 × 2 pt, the level of consistency with Planck remains roughly the same. This results from the preference by hear kind for somewhat higher values of q, as seen in Fig.3. Figure 13 directly compares the Sand Ω_m constraints from these and other two-point function combinations, assuming ΛCDM. We note that for consistency with our analysis, we vary the sum of the neutrino masses and impose the priors shown in Table II when generating the Planck primary CMB constraints shown in this figure.

V. SUMMARY

We have presented cosmologicaconstraints from an analysis of two-pointcorrelation functions between measurements of galaxy positions and galaxy lensing from DES Y3 data and CMB lensing measurements from SPT and Planck. Our main cosmological constraints are summarized in Table I.

The high signal-to-noise of the CMB lensing crosscorrelation measurements sing DES Y3, SPT-SZ and Planck data enables powerful robustnesstests of our cosmologicalconstraints. The results of several of these tests are shown in Fig. 13. We summarize the main findings and the summarize the main findings and the summarize the main findings are shown in Fig. 13. We summarize the main findings are shown in Fig. 13. of these tests below:

- (i) The goodness of fit of Λ CDM to the 5 × 2 pt data vector is acceptable (p \(\frac{1}{4} \) 0.062), and the corresponding parameter constraints are consistenth those from hember imeasurements by Planck.
- (ii) Using only cross-correlations between DES and CMB lensing, we obtain constraints on Sthat are comparable in precision and consistent with the baseline 5 × 2 ptresults. This result suggests that additive systematics are not significantly impacting the 5 × 2 pt cosmological constraints.
- from galaxy overdensities) yields constraints in agreementwith the baseline results. This result suggeststhat potential systematicsimpacting the DES galaxy samples, as well as modeling of galax bias, are not significantly biasing the 5 × 2 pt cosmological constraints.
- (iv) The cosmologicabonstraints from two-poinfunctions of MAGLIM galaxy overdensity measurements and CMB lensing are generally consistewith the baseline 5 × 2 ptanalysis. This result suggests that not significantly biasing the 5 × 2 ptcosmological constraints. We do, however, observe a lowsignificance increase in \$\\$ when considering only those two-point functions that do not involve and hkcmbkcmbi of the $h \delta_q \delta_q i \not = h \delta_q \kappa_{CMB} i$

- constraints, and is not present when considering $hδ_gδ_gi þ hδ_gκ_{CMB}i$ alone.
- (v) Without priors on shear calibration the cosmological constraintson S₈ from 5 × 2 pt are in good agreement with the baseline 5 × 2 pt results. The data calibrate the shear bias parametersat the 5%–10% level, and yield constraints consistent with our nominal priors. These results suggest that shear calibration biases are not significantly impacting the 5 × 2 pt cosmological constraints.
- The constraints on Ω_n from the different analysis variations are generally consistent. Although the analysis of haccmbi b hγtκcmbi b hκcmbκcmbi prefers a somewhat lower value of this combination of probes is statistically consistent with 3×2 pt.

The cosmological constraints from the 3×2 pt5 $\times 2$ pt, and 6 × 2 pt analyses therefore appear remarkably robust to possible systematic biases.

Assessing the consistency between ouconstraint on Λ CDM and those of Planck, we find that the 5 × 2 pt and 6 × 2 pt constraints are statistically consistent with Planck at the 1.4σ level, as assessed using the fulmultidimensional posteriors from these measurements As seen in Fig. 13, however, essentially all combinations of two point functions that we consider prefer lower S₈ values than between some of these measurements.

We have also investigated possible issues with the analysis of alternate lens galaxy samples, namely the high-redshift MAGLIM galaxies and the REDMAGIC galaxies. Evidence for biases when analyzing correlation f unctions measured with these samples was found previously in [20,19,40,4]. The CMB lensing cross-correlations considered here provide a powerful way to probe the sourcesof these biases. In the context of ACDM, our analysis of CMB lensing cross-correlations suggestsa possible problem in the modeling of by at high redshift (iii) Using only gravitational lensing (i.e., no information for the MAGLIM galaxies, and possibly the REDMAGIC galaxies as well. At the same time, the home measurements with REDMAGIC suggesta possible observational systematic that impacks DMAGIC galaxy clustering across all redshifts. This interpretation is supported by tests with an alternate REDMAGIC galaxy sample in [19]. In the context of wCDM, the 3 × 2 pt measurementswith REDMAGIC have previously shown to yield constraints inconsistentwith the MAGLIM analysis, and a preference for surprisingly less negative w. We show that analysis of shear systematics and modeling of galaxy lensing are in h h $\delta_g \kappa_{CMB}$ i $\delta_g \kappa_{CMB}$ i $\delta_g \kappa_{CMB}$ i (i.e., two-point functions) tions between DES and CMB lensing, excluding galaxy clustering) measured with EDMAGIC yields cosmological constraints that are in better agreement with GLIM, and do not show a strong preference for w > -1Finally, we galaxy lensing. This shift is driven by the intersection ote that while the analyses presented here suggest possible interpretations of the Ks bias, more work with current and

future DES data is needed to clarify the true source of thisat Urbana-Champaign, the Kavli Institute of Cosmological systematic uncertainty.

As the data volume and quality from cosmological surveys continue to improve, we expect similar crosscorrelation analyses between galaxy surveysand CMB lensing measurements to play an importantole in constraining late-time large scale structure. Excitingly, we expect constraints from such measurements improve dramatically in the very near future with Year 6 data from Tecnológico and the Ministrio da Ciência, Tecnologia e DES and new CMB lensing maps from SPT-3G [66] and Inovação, the Deutsche Forschungsgemeinschaftd the AdvACT [67]. These measurements should help to provideollaborating Institutions in the Dark Energy Survethe a clearer picture of any possibletension. Looking farther forward, cross-correlationsetween surveys such ashe Vera Rubin Observatory Legacy Survey of Space and Tincambridge, Centro de Investigaciones Energéticas, [68,69], the Nancy Grace Roman Space Telescope [70], thredioambientales y Tecnológicas-Madrithe University ESA Euclid mission [71], Simons Observatory [72]and CMB-S4 [73] will enable significantly more powerful crossconsortium, the University of correlation studies that will deliver some of the most precisedgenössischeTechnischeHochschule (ETH) Zürich, and accurate cosmological constraints that will allow

ACKNOWLEDGMENTS

National Science Foundation (NSF) through the grant OPPssociated Excellence Cluster University of 1852617. Partial support is also provided by the Kavli Institute of Cosmological Physics at the University of Chicago. Argonne National Laboratory's work was supported by the U.S. Department of Energy, Office of Science, Office of High Energy Physics, under contract No. DE-AC02-06CH11357. Work at Fermi National Accelerator Laboratory, a DOE-OS, HEP User Facility managed by the Fermi Research Alliance, LLC, was supported under Contract No. DE-AC02-07CH11359. The Melbourne authors acknowledgesupport from the Australian Research Council's Discovery Projects scheme National Science Foundation The DES data manage-(DP210102386). The McGill authors acknowledge fundingment system is supported by the National Science from the Natural Sciences and Engineering Research Council of Canada, Canadian Institute for Advanced et technologies. The CU Boulder group acknowledges supportfrom NSF GrantNo. AST-0956135.The Munich group acknowledges the support by the ORIGINS Cluster 2016-0597, and No. MDM-2015-0509, some of which (funded by the Deutsche Forschungsgemeinschaft include ERDF funds from the European Uniorh. F. A. E. (DFG, German Research Foundation) under Germany's Excellence Strategy—EXC-2094-390783311), the MaxPlanck-Gesellschaftaculty Fellowship Programand the Ludwig-Maximilians-Universität München. J. V. acknowledges support from the Sloan Foundation. Funding for the DES Projects has been provided by the U.S. Departmentof Energy, the U.S. National Science Foundation, the Ministry of Science and Education of Spain, the Science and Technology Facilities Council the United Kingdom, the Higher Education Funding Council for England, the National Center for Supercomputing Applications athe University of Illinois

Physics at the University of Chicago, the Center for Cosmology and Astro-Particle Physics athe Ohio State University, the Mitchell Institute for Fundamenta Physics and Astronomy at Texas A&M University, Financiadora de Estudos e Projetos, Fundação Carlos Chagas Filho de Amparo à Pesquisa do Estado do Rio de Janeiro, Conselho Nacional de Desenvolvimento Científico e Collaborating Institutions are Argonne National Laboratory, the University of California at Santa Cruz, the University of of Chicago, University College London, the DES-Brazil Edinburgh, the Fermi National Accelerator Laboratorythe University of us to continue stress-testing the concordance ΛCDM modifinois at Urbana-Champaigrthe Institut de Ciències de l'Espai (IEEC/CSIC), the Institut de Física d'Altes Energies, Lawrence Berkeley National Laboratory, the The South Pole Telescope program is supported by the Ludwig-Maximilians Universität München and the Michigan, NFS's NOIRLab, the University of Nottingham, The Ohio State University, the University of Pennsylvania, the University of Portsmouth\$LAC National Accelerator Laboratory Stanford University the University of Sussex, Texas A&M University, and the OzDES Membership Consortium. Based in part on observationsat Cerro Tololo Inter-American Observatory at NSF's NOIRLab (NOIRLab Prop.ID 2012B-0001; PI: J. Frieman), which is managed by the Association of Universities for Research in Astronomy (AURA) under a cooperative agreement with Foundation under Grants No. AST-1138766 and No. AST-1536171. The DES participants from Spanish researchand the Fonds de recherche du Quúbec Nature institutions are partially supported by MICINN under grants ESP2017-89838, No. PGC2018-094773. No. No. PGC2018-102021No. SEV-2016-0588,No. SEVis partially funded by the CERCA program of the Generalitat de Catalunya. Research leading to these results has received funding from the European Research Council under the European Union's Seventh Framework Program (FP7/2007-2013) including ERC grant agreements No. 240672, No. 291329, and No. 306478. We acknowledge support from the Brazilian Instituto Nacional de Ciência e Tecnologia (INCT) do e-Universo (CNPg grant No. 465376/2014-2). This manuscript has been authored by Fermi Research Alliance LLC under Contract No. DE-AC02-07CH11359 with the U.S. Department of Energy, Office of Science, Office of High Energy Physics. We

gratefully acknowledge the computing resources provided on Crossover (and/or Bebop and/or Swing and/or Blues), a high-performance computing cluster operated by the Laboratory Computing Resource Center at Argonne National Laboratory.

APPENDIX A: PARAMETER PRIORS

In Table II we list the priors used in our analysis.

TABLE II. Prior values for cosmological and nuisance param eters included in our modelFor the priors, U1/2a; bindicates a function at value a, which effectively means that the parameter parameters which degrades the parameter on straints to fixed at a. Note that the fiducial lens sample is the first 4 bins of the extent. In the case of the particular nonlinear bias MAGLIM sample. The two high-redshift MAGLIM bins and the the fiducial analysis.

Parameter	Prior				
Ω_{m}	U½0.1; 0.9				
$A_s \times 10^9$	U½0.5; 5.0				
n _s	U½0.87; 1.07 U½0.03; 0.07				
Ω _b	U½0.55; 0.91				
$\Omega_{\rm v}$ h ² × 10 ⁴	U½6.0; 64.4				
·	,				
a ₁ a ₂	U½-5.0; 5.0 U½-5.0; 5.0				
η_1	U½-5.0; 5.0				
η_2	U½-5.0; 5.0				
b _{ta}	U½0.0; 2.0				
MAGLIM					
b ¹⁶	U½0.8; 3.0				
b ₁ ¹⁶	U½0.67; 3.0				
b ₂ ¹⁶	U½−4.2; 4.2				
b ₂ ¹⁶ C ₁ ¹⁶	δὄ0.42Þδὄ0.3Þδὅ1.76Þδὅ1.94Þδὅ1.56Þ,				
	δð2.96Þ				
$\Delta_z^{16} \times 10^2$	N ½-0.9; 0.7N ½-3.5; 1.1N ½-0.5; 0.6,				
_1 6	N ½-0.7; 0.6N ½0.2; 0.7N ½0.2; 0.8				
σ_z^{16}	N ½0.98; 0.062), ½1.31; 0.093, N ½0.87; 0.054), ½0.92; 0.05,				
	N ½1.08; 0.067N ½0.845; 0.073				
	11 /21.00, 0.001, /20.010, 0.010				
REDMAGIC b ¹⁵	U½0.8; 3.0				
b ₁ ⁵	U½0.67; 2.52				
b ₁ ¹⁵	U½-3.5; 3.5				
C.15	δὄ0.62Þδő-3.04Þδő-1.32Þδδ2.5Þδδ1.94Þ				
C_1^{15} $\Delta_z^{15} \times 10^2$	N ½0.6; 0.4N ½0.1; 0.3N ½0.4; 0.3,				
_2	N ½-0.2; 0.5N ½-0.7; 1.0				
σ_z^{14}	δδ1Þδδ1Þδδ1Þδδ1ÞΝ 1/21.23; 0.054				
METACALIBRATI	ON				
$m^{14} \times 10^3$	N ½-6.0; 9.1N ½-20.0; 7.8N ½-24.0; 7.6,				
	N ½-37.0; 7.6				
$\Delta_z^{14} \times 10^{-2}$	N ½0.0; 1.8N ½0.0; 1.5N ½0.0; 1.1,				
	N ½0.0; 1.7				

APPENDIX B: ADDING SMALL-SCALE INFORMATION WITH NONLINEAR **GALAXY BIAS**

describe the relationship between the galaxy overdensity and the underlying matter field. At small scales, this description of galaxy biasing is known to break down. The breakdown in linear galaxy bias drives our choice of angular scales used to analyzing the hacmai correlation, as described in Paper I. By adopting a higher-orderbias model, it is possible to include smaller angular scales in the cosmological analysis uniform prior between a and b, while N ½a; b indicates a Gaussad potentially improve parameter constraints. At the same prior with mean a and standard deviation b. δδαÞ is a Dirac Deltine, a more complex bias modehecessitates more free REDMAGIC sample are shown in gray to indicate they are not part of eters is equal to the number of lens galaxy tomographic bins, which is four for our baseline analysis. We now consider the parameterconstraints from 5 × 2 pt using the nonlinear galaxy bias model described in [19].

Our baseline analysis adopts a linear galaxy bias model to

The constraints from this analysis are presented in Fig. 14. We find that adopting a nonlinear description of galaxy bias (and using the corresponding selection of angular scales) improves the precision of the constraints on both Ω_0 and S_0 by roughly 10%. Thus, the inclusion of the small-scale measurements in the nonlinear bias analysis compensates for the increase in model freedom.

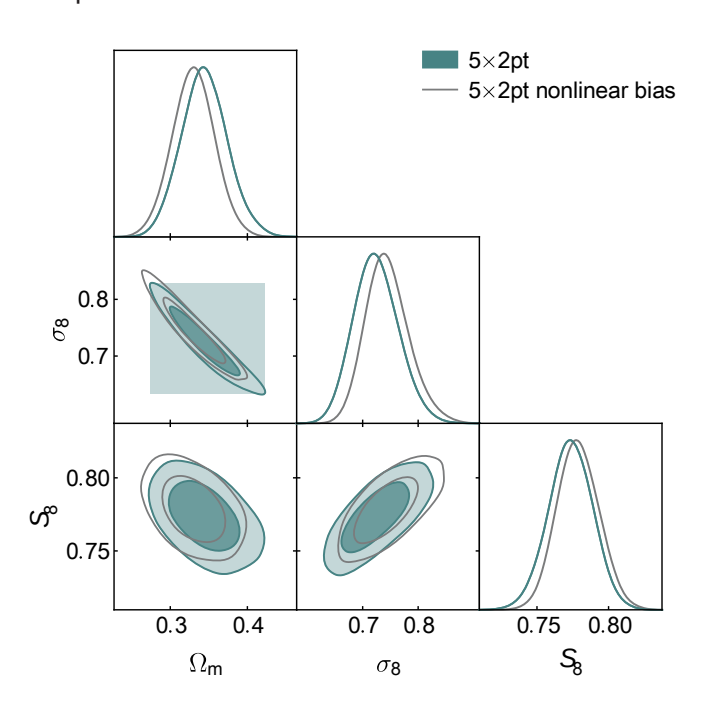


FIG. 14. Parameter constraints obtained when using a nonlinear galaxy bias model to analyze the 5 × 2 pt data vector(gray) compared to our baseline 5 × 2 pt analysis (teal), which adopts a linear bias model. The nonlinear bias analysis can be used to fit smaller scales of measured correlation functions esulting in improved constraints.

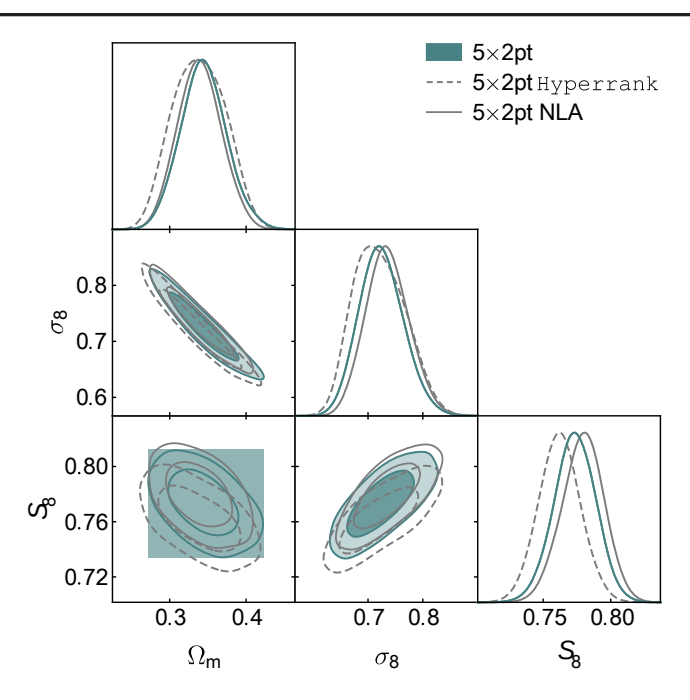


FIG. 15. Parameter constraints obtained when using alternative prescriptions for modeling photometric redshift biases and intrinsic alignments. The teal curves show our baseline results, while the gray dashed curves show results assume in a light manufacture and the curves show are shown our baseline results, while the gray dashed curves show results assume in a light manufacture and the curves show our baseline results, while the gray dashed curves show results assume in a light manufacture and the curves are curves as the curves are curves are curves as the curves are curves are curves as the curves are curves as the curves are curves are curves as the curves are curves are curves are curves are curves as the curves are curves are curves are curves are curves are curves are curves as the curves are c calibrating the source galaxy redshift distributions, and the gray solid curves show results assuming the NLA intrinsic alignment mode (rather than the baseline TATT model). In both cases, there are minimal shifts relative to our baseline results.

APPENDIX C: ALTERNATIVE REDSHIFT CALIBRATION AND IA MODEL

Our baseline analysis assumes that certainties in the source galaxy redshiftdistributions are characterized by shift and stretch parameters described in [41,42].An alternative approach to characterizing the uncertainties in the redshift distributions is YPERRANK, described in [44]. distributions, HYPERRANK provides a way to sample over realizations of the full posteriors on these distributions. Repeating our analysis of the 5 × 2 pt data using this

alternative redshift uncertainty prescription yields the constraints shown in Fig. 15. Although there is a small shift in S₈, it is well within our uncertainties.

The intrinsic alignment (IA) model that we adopt in our baseline analysis is TATT [TATT, 39]. In Fig. 15, we show the results of instead adopting the nonlinearalignment model [NLA, 74]. The NLA model is more restrictive than Rather than attempt to parameterize biases in the redshift. TATT in the sense that the latter becomes equivalent to the former in the limit that $a_2 \frac{1}{4} p_2 \frac{1}{4} b_{ta} \frac{1}{4} 0$. We find that switching to NLA results in minimal changes to the parameter constraints from 5 × 2 pt.

^[1] C. Heymans, T. Tröster, M. Asgari et al., Astron. Astrophys[8] M. Raveri and W.Hu, Phys.Rev.D 99, 043506 (2019). 646, A140 (2021).

^[2] T. Hamana, M. Shirasaki, S. Miyazaki et al., Publ. Astron. Soc. Jpn. 72, 16 (2020).

^[3] T. M. C. Abbott, et al. (DES Collaboration), Phys. Rev. D 98, 043526 (2018).

^[4] T. M. C. Abbott, et al. (DES Collaboration), Phys. Rev. D 105, 023520 (2022).

^[5] R. A. Battye, T. Charnock, and A. Moss, Phys. Rev. D 91, 103508 (2015).

^[6] N. MacCrann, J. Zuntz, S. Bridle, B. Jain, and M. R. Becker, Mon. Not. R. Astron. Soc. 451, 2877 (2015).

^[7] M. Raveri, Phys. Rev. D 93, 043522 (2016).

^[9] N. Aghanim et al. (Planck Collaboration), Astron. Astrophys.641, A6 (2020).

^[10] A. Krolewski, S. Ferraro, and M. White, J. Cosmol. Astropart. Phys. 12 (2021) 028.

^[11] N. C. Robertson, D. Alonso, J. Harnois-Déraps et al., Astron. Astrophys. 649, A146 (2021).

^[12] C. Chang, Y. Omori, E. J. Baxter et al., preceding paper, Phys.Rev.D 107, 023530 (2023).

^[13] M. White, R. Zhou, J. DeRose et al., J. Cosmol. Astropart. Phys.02 (2022) 007.

^[14] C. Chang, M. Wang, S. Dodelson et al., Mon. Not. R. Astron. Soc. 482, 3696 (2019).

- [15] J. E. Carlstrom, P. A. R. Ade, K. A. Aird et al., Publ. Astron 45] N. MacCrann, M. R. Becker, J. McCullough et al., Mon. Soc. Pac. 123, 568 (2011). Not. R. Astron. Soc. 509, 3371 (2022).
- [16] P. A. R. Ade et al. (Planck Collaboration), Astron. Astrophys.536, A1 (2011).
- [17] Y. Omori, R. Chown, G. Simard et al., Astrophys. J. 849, 124 (2017).
- [18] Y. Omori, E. J. Baxter, C. Chang et al., this issue, Phys. R 88 M. Rodríguez-Monroy, N. Weaverdyck, J. Elvin-Poole D 107, 023529 (2023).
- [19] S. Pandey E. Krause, J. DeRose et al. Phys. Rev. D 106, 043520 (2022).
- 106, 103530 (2022).
- Astron. Soc. 461, 4099 (2016).
- [22] D. Kirk, Y. Omori, A. Benoit-Lévy et al., Mon. Not. R. Astron. Soc. 459, 21 (2016).
- [23] T. Giannantonio P. Fosalba, R. Cawthon et al., Mon. Not. R. Astron. Soc. 456, 3213 (2016).
- [24] E. J.Baxter, S. Raghunathan, T. M. Crawford et al., Mon. Not. R. Astron. Soc. 476, 2674 (2018).
- 100,043501 (2019).
- [26] Y. Omori, E. J.Baxter, C.Chang et al., PhysRev. D 100, 043517 (2019).
- [27] T. M. C. Abbott, F. B. Abdalla, A. Alarcon et al., Phys. Rev[57] C. Sánchez, J. Prat, G. Zacharegkas et al., Phys. Rev. D 105 D 100, 023541 (2019).
- [28] M. S. Madhavacheriland J. C. Hill, Phys. Rev. D 98, 023534 (2018).
- [29] B. Flaugher, Int. J. Mod. Phys. A 20, 3121 (2005).
- [30] B. Flaugher, H. T. Diehl, K. Honscheid et al. (DES Collaboration), Astron. J. 150, 150 (2015).
- [31] I. Sevilla-Noarbe, K. Bechtol, M. Carrasco Kind et al., Astrophys.J. Suppl. Ser. 254, 24 (2021).
- [32] A. Porredon et al. (DES Collaboration), Phys. Rev. D 103,[62] A. Vallinotto, Astrophys.J. 759, 32 (2012). 043503 (2021).
- [33] M. Gatti, E. Sheldon, A. Amon et al., Mon. Not. R. Astron. Soc. 504, 4312 (2021).
- [34] E. Krause, X. Fang, S. Pandey et al., arXiv:2105.13548.
- [35] D. N. Limber, Astrophys.J. 117, 134 (1953).
- [36] A. Lewis, A. Challinor, and A. Lasenby, Astrophys. J. 538 473 (2000).
- [37] R. Takahashi, M. Sato, T. Nishimichi, A. Taruya, and M. Oguri, Astrophys.J. 761, 152 (2012).
- [38] X. Fang, E. Krause, T. Eifler, and N. MacCrann, J. Cosmol. Astropart. Phys. 05 (2020) 010.
- [39] J. A. Blazek, N. MacCrann, M. A. Troxel, and X. Fang, Phys.Rev.D 100, 103506 (2019).
- [40] J. Elvin-Poole, N. MacCrann et al., arXiv:2209.09782.
- [41] J. Myles, A. Alarcon, A. Amon et al., Mon. Not. R. Astron. [70] O. Doré, C. Hirata, Y. Wang etal., arXiv:1904.01174. Soc. 505, 4249 (2021).
- [42] M. Gatti, G. Giannini, G. M. Bernstein et al., Mon. Not. R. [72] P. Ade, J. Aguirre, Z. Ahmed et al., J. Cosmol. Astropart. Astron. Soc. 510, 1223 (2022).
- [43] R. Cawthon et al. (DES Collaboration), Mon. Not. R. Astron. Soc. 513, 5517 (2022).
- [44] J. P. Cordero, I. Harrison, R. P. Rollins et al., Mon. Not. R.[74] S. Bridle and L. King, New J. Phys. 9, 444 (2007). Astron. Soc. 511, 2170 (2022).

- - [46] N. MacCrann, J. Blazek, B. Jain, and E. Krause, Mon. Not. R. Astron. Soc. 491, 5498 (2020).
 - [47] M. Jarvis, G. Bernstein, and B. Jain, Mon. Not. R. Astron. Soc. 352, 338 (2004).
- et al., Mon. Not. R. Astron. Soc. 511, 2665 (2022).
- [49] J. Prat, J. Blazek, C. Sánchez etal., Phys. Rev. D 105, 083528 (2022).
- [20] A. Porredon, M. Crocce, J. Elvin-Poole et al., Phys. Rev. [20] A. Amon, D. Gruen, M. A. Troxel et al., Phys. Rev. D 105, 023514 (2022).
- [21] E. Baxter, J. Clampitt, T. Giannantonio et al., Mon. Not. R.[51] L. F. Secco, S. Samuroff, E. Krause et al., Phys. Rev. D 105, 023515 (2022).
 - [52] M. Bartelmann and P. Schneider, Phys. Rep. 340, 291 (2001).
 - [53] O. Friedrich, F. Andrade-Oliveira, H. Camacho et al., Mon. Not. R. Astron. Soc. 508, 3125 (2021).
 - [54] C.-H. Lin, J. Harnois-Déraps, T. Eifler, T. Pospisil, R. Mandelbaum, A. B. Lee, and S. Singh, Mon. Not. R. Astron. Soc. 499, 2977 (2020).
- [25] Y. Omori, T. Giannantonio, A. Porredon et al., Phys. Rev. [35] J. Zuntz, M. Paterno, E. Jennings et al., Astron. Comput. 12, 45 (2015).
 - [56] W. J. Handley, M. P. Hobson, and A. N. Lasenby, Mon. Not. R. Astron. Soc. 453, 4384 (2015).
 - 083529 (2022).
 - [58] C. Doux, E. Baxter, P. Lemos et al., Mon. Not. R. Astron. Soc. 503, 2688 (2021).
 - [59] M. Raveri and C. Doux, Phys. Rev. D 104, 043504 (2021).
 - [60] S. Pandey, E. Krause, B. Jain et al., Phys. Rev. D 102, 123522 (2020).
 - [61] C. Hirata and U. Seljak, Mon. Not. R. Astron. Soc. 343, 459 (2003)

 - [63] E. Schaan, E. Krause, T. Eifler, O. Doré, H. Miyatake, J. Rhodes, and D. N. Spergel, Phys. Rev. D 95, 123512 (2017).
 - [64] D. Baumann, S. Ferraro, D. Green, and K. M. Smith, J. Cosmol.Astropart.Phys.05 (2013) 001.
 - [65] V. Desjacques, D. Jeong, and F. Schmidt, Phys. Rep. 733, 1 (2018).
 - [66] J. A. Sobrin, A. J. Anderson, A. N. Bender et al., Astrophys. J. Suppl. Ser. 258, 42 (2022).
 - [67] S. W.Henderson, R. Allison, J. Austermann et al., Low Temp.Phys.184,772 (2016).
 - [68] Ž. Ivezić, S. M. Kahn, J. A. Tyson et al., Astrophys. J. 873, 111 (2019).
 - [69] P. A. Abell, J. Allison et al. (LSST Science Collaboration), arXiv:0912.0201.

 - [71] R. Laureijs, J. Amiaux, S. Arduini et al., arXiv:1110.3193.
 - Phys.02 (2019) 056.
 - [73] K. N. Abazajian, P. Adshead, Z. Ahmed et al., arXiv:1610 .02743.